CONCEPTUAL DESIGN ORIENTED WING STRUCTURAL ANALYSIS AND OPTIMIZATION

by

May Yuen Lau

A thesis submitted in partial fulfillment of the
requirements for the degree of

Master of Science
in Aeronautics and Astronautics

University of Washington

1996

Approved by _____
Chairperson of Supervisory Committee

Program Authorized
to Offer Degree Aeronautics and Astronautics

Date December 11, 1996

Master's Thesis

In presenting this thesis in partial fulfillment of the requirements for a Master's degree at the University of Washington, I agree that the Library shall make its copies freely available for inspection. I further agree that extensive copying of this thesis is allowable only for scholarly purposes, consistent with "fair use" as prescribed in the U.S. Copyright Law. Any other reproduction for any purposes or by any means shall not be allowed without my written permission.

Signature _____

Date 12/4/96

TABLE OF CONTENTS

LIST OF FIGURES

LIST OF TABLES

CHAPTER 1

INTRODUCTION

Airplane optimization has always been the goal of airplane designers. In the conceptual design phase, a designer's goal could be tradeoffs between maximum structural integrity, minimum aerodynamic drag, or maximum stability and control, many times achieved separately. Bringing all of these factors into an iterative preliminary design procedure was time consuming, tedious, and not always accurate. For example, the final weight estimate would often be based upon statistical data from past airplanes. The new design would be classified based on gross characteristics, such as number of engines, wingspan, etc., to see which airplanes of the past most closely resembled the new design.(Ref. 1) This procedure works well for conventional airplane designs, but not very well for new innovative designs.

With the computing power of today, new methods are emerging for the conceptual design phase of airplanes. Using finite element methods, computational fluid dynamics, and other computer techniques, designers can make very accurate disciplinary analyses of an airplane design. These tools are computationally intensive, and when used repeatedly, they consume a great deal of computing time. In order to reduce the time required to analyze a design and still bring together all of the disciplines (such as structures, aerodynamics, and controls) into the analysis, simplified design computer analyses are linked together into one computer program. These design codes

are very efficient for conceptual design. One such program, called ACSYNT (Ref. 2-4), is being developed by the NASA Ames Research Center.

The work in this thesis is focused on a finite element based conceptual design oriented structural synthesis capability (CDOSS) tailored to be linked into ACSYNT. CDOSS and ACSYNT exchange data. CDOSS automatically generates a mesh for a finite element model for airplane wings from the geometry data received from ACSYNT. The structural analysis of the finite element model includes stress analysis with calculation of deformations and buckling stresses. Optimality criteria based structural optimization is used in CDOSS. Weight is estimated by summing the weight of the individual elements corrected for manufacturing information.

Shape variation is also very important in conceptual design. Changes in local elements as well as overall planform should be part of the optimization process. The structural analysis is done by generating a mesh for a finite element model. The difficulty with finite element models is that greater accuracy is obtained by using a finer mesh. However, a finer mesh requires more computing time. Optimization is performed using constraints on deformations, stresses, and buckling. The focus of this work is to perform these tasks efficiently and accurately for conceptual design.

The outline of this work is as follows: in chapter 2 the finite element modeling and analysis is discussed. Chapter 3 focuses on the wing shape parameterization and configuration. In chapter 4, the behavior constraints for optimization are described. Chapter 5 has a discussion of the structural weight evaluation and optimization

algorithms. In chapter 6, the test case of a fighter type wing is discussed. Information concerning the use of CDOSS is in the appendix.

CHAPTER 2

FINITE ELEMENT WING MODELING AND ANALYSIS

2.1 Introduction

The modeling for wing box finite element analysis is described in this chapter. The construction of the wing and the elements used will be discussed. Sensitivities with respect to shape will be described. Finite element analysis of the wing model and calculation of stresses and deformations will be covered. A brief discussion of the structural vibration modes will also be included in this chapter. Load cases and interpolation of loads to the finite element mesh will be described.

2.2 Wing Construction

The wing box is constructed with cover skins, spars and ribs. Membrane (plane stress) elements and truss elements are use to model the parts of the wing box. Spars and ribs are modeled with two caps and a shear web between the caps. Cover skins and webs are modeled using membrane elements in plane stress. Truss (rod) elements are used for spar and rib caps. Figure 1 illustrates the wing box model. The cover skin is made of thin membrane elements. The spars (or ribs) are modeled with caps and a thin shear web. Skin membrane elements can take tension, compression, and shear stresses. Web membrane elements are in shear only and cannot take tensile or compressive

stresses. The rod (truss) elements are in tension or compression and cannot take bending stresses. Thus, the wing skin and spar caps resist resist transverse shear. Vertical spacers (rods) are placed at all nodes between the upper and lower skin. The spacers are necessary to keep the skins from collapsing onto each other.

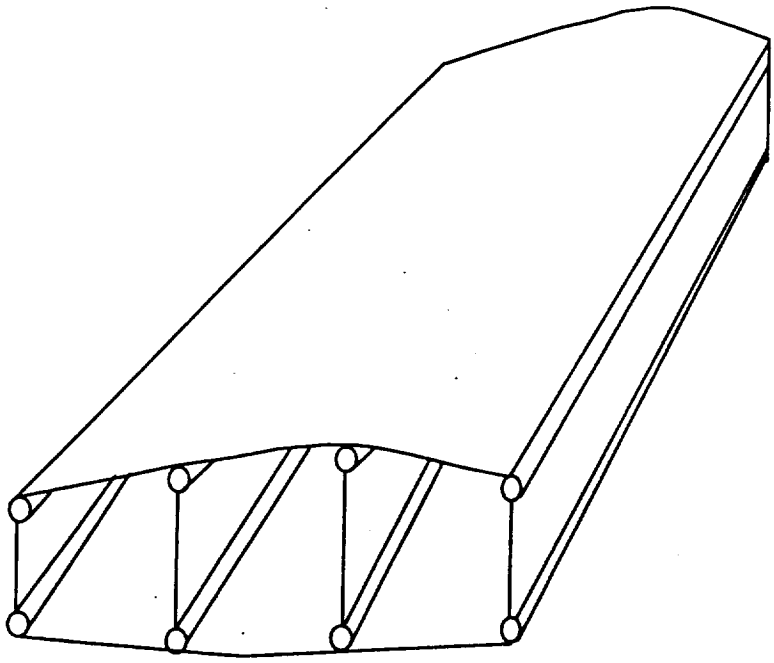

Figure 1. Wing Box Model

2.3 Elements

The elements chosen are simple and allow for faster computation and closed form, explicit analytic sensitivity analysis. (Ref. 5) The rod elements are simple linear elements. The membranes are broken into constant strain triangular (CST) elements. All elements have constant stress throughout the element which causes stress discontinuities where elements meet. In parts, such as the wing skin, the stresses can be smoothed to get a continuous change of stress values from root to tip. For a more refined grid, "dummy" elements are used to support nodes which are not on actual ribs or spars. In figure 2, a portion of the wing with three ribs and 3 spars has 9 nodes and the elements are quite large. With the addition of two "dummy" ribs and two "dummy" spars, the same section of the wing now has 25 nodes. The length of each truss element is halved and the area of each membrane element is quartered. "Dummy" spars and "dummy" ribs are used solely to create a better, more refined mesh. They do not provide any structural strength. To ensure that they neither add to strength or weight, these elements are given very small thickness (1% of that of real elements) and we can add nodes without causing singularities in the stiffness matrix.(Ref. 6) The real elements and "dummy" elements are treated the same way in the analytic differentiation with respect to shape.

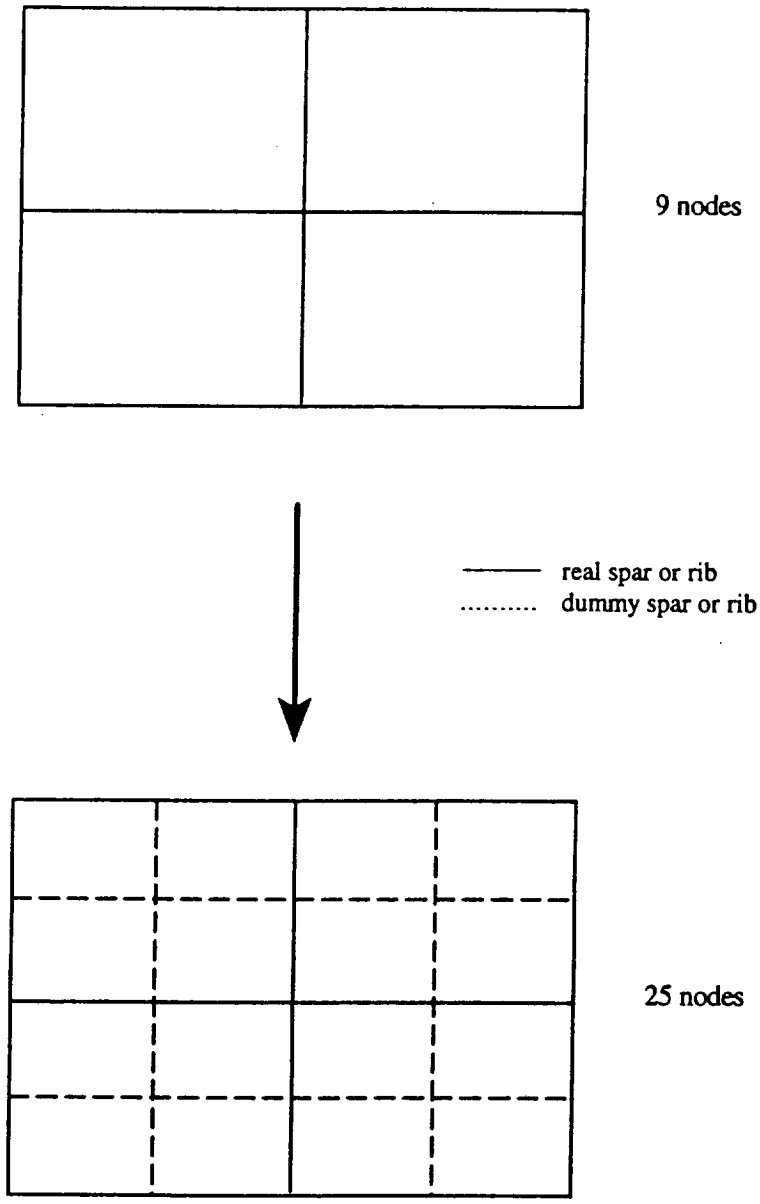

Figure 2. Mesh Refinement

2.4 Sensitivities

Structural behavior sensitivities with respect to shape design variables is important for shape optimization. Sensitivities are used to calculate gradients and to construct approximate constraint functions and objective functions. Since we used simple finite elements in modeling the wing, the mass and stiffness matrices are explicit and algebraic in nature. This allows us to differentiate the basic structural equations explicitly with respect to any design variable. We obtain sensitivities in a closed, explicit analytic form without numerical integration. (Ref. 7)

2.5 Deformations

For a static structural system, the governing equation is given by

$$[K]\{u\} = \{F\}$$

where [K] is the banded global stiffness matrix, {u} is the global displacements vector, and {F} is the nodal loads vector. We solve for the displacement vector using a decomposition technique and skyline solver of Ref. 8.

2.6 Stresses

Individual finite element stresses are calculated using the global displacements found previously. For rod elements, we use Hook's stress/strain law to find the axial

stress in the element. (Ref. 9) The change in the length of the rod is found from subtracting the displacements of the two ends. Strain is the change in length divided by the original length of the rod. Then using Hook's law, $\sigma=E\varepsilon$, we find element stress. The local strains can be transformed into global strains in order to obtain global stresses. For the CST membrane elements, the procedure is similar. The stress is no longer a scalar. It is a vector of σ_{xx}, σ_{yy}, and σ_{xy} and E is a matrix of constitutive properties.

2.7 Vibration Modes

The vibration modes are important when analyzing a dynamic structural system. In the case of wing structures, they are required for flutter and dynamic response analysis. To find the natural frequencies and the vibration modes, we use an eigenvalue function method. The governing equation for undamped simple harmonic motion is

$$[K - \omega^2 M]\{\phi\} = \{0\}$$

K is the global stiffness matrix, ω is the natural frequency, M is the global mass matrix, and ϕ is the mode shape. For a non-trivial solution, the determinant of $[K - \omega^2 M]$ must be equal to zero. The eigenvalues of the system are equal to ω^2 and corresponding eigenvectors are mode shapes.

2.8 Loads

There is a large number of loads that can be applied to a wing. These loads come from many different sources. Some possibilities are lumped mass from external stores or tanks, uniform pressure loads, distributed loads, loads from control surface, or aerodynamic loads. These loads must be applied carefully to the planform of the finite element model. For a finite element model, all loads must be applied at the nodes. Figure 3 illustrates how a uniformly distributed load is transformed into concentrated loads at the points where there is structural support. Nodes where "dummy" spars and "dummy" ribs intersect are called "floating" nodes. Loads cannot be applied at "floating" nodes where no real structure exists to support the load. We must use interpolation to "move" loads to nodal points while keeping the load distribution and force resultants as close to the original as possible.

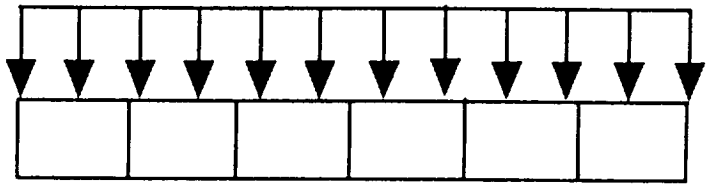

Distributed Load (lb/in)

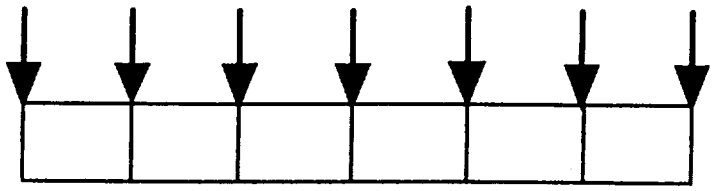

Interpolated Load (lbs)

(Equivalent concentrated loads at nodal points)

Figure 3. Load Transformation

2.9 Aerodynamic Load Transformation

Aerodynamic analysis of a wing utilizes a grid of points similar to the grid used in the structural analysis. Usually the points of these two grids will not match one another. In order to use the aerodynamic load distribution in the structural analysis, the loads must be transformed to the structural grid. One method is to use energy principles and the concept of work. Deformations can be represented by a series of polynomial functions or by shape functions. A description of both types of function transformation follow. A comparison of results using the Chebychev functions and the shape functions will be presented in chapter 6.

2.9.1 Polynomial Functions

Displacements are represented by a series of polynomial functions.

$$w(x,y) = f_1(x,y)q_1+f_2(x,y)q_2+ \ldots +f_n(x,y)q_n$$

The series is evaluated at all structural points and aerodynamic points. All the grid points are transformed to a unit box to help prevent ill-conditioning in matrices. The two matrices, [Ws] and [Wa], can be created where each row of [Ws] consists of the polynomials, f_n, evaluated at a structural point and each row of [Wa] consists of the polynomials evaluated at an aerodynamic point. Requiring that the work done by each system is equal results in the following matrix equation.

$$\{Fs\}^T[Ws]\{q\} = \{Fa\}^T[Wa]\{q\}$$

{Fs} and {Fa} are vectors of the forces at the structural points and aerodynamic points respectively. The equation above must hold for any vector {q}. The following derivation results in a relationship to find {Fs}, the equivalent forces on the structural grid.

$$\{Fs\}^T[Ws] = \{Fa\}^T[Wa]$$

$$[Ws]^T\{Fs\} = [Wa]^T\{Fa\}$$

$$[Ws][Ws]^T\{Fs\} = [Ws][Wa]^T\{Fa\}$$

Let

$$[A] = [Ws][Ws]^T$$

$$[B] = [Ws][Wa]^T$$

where [A] is now a square, symmetric matrix.

$$[A]\{Fs\} = [B]\{Fa\}$$

$$\{Fs\} = [A]^{-1}[B]\{Fa\}$$

Using the above equation, the equivalent force on the structural points can be found.

The polynomial functions chosen for this work were Chebychev polynomials. The Chebcychev polynomials are formed in the following manner.

$$T_1(x) = 1.0$$

$$T_2(x) = x$$

$$T_3(x) = 2x^2\text{-}1$$

$$T_n(x) = 2xT_{n-1}(x)-T_{n-2}(x)$$

The polynomial functions are evaluated for the x and y coordinates for both the structural grid points and the aerodynamic grid points. Then the matrices [Ws] and [Wa] can be created, where a typical shape function $f_r(x,y)$ is given by

$$f_r(x,y) = T_i(x)*Tj(y)$$

Chebychev polynomials use high order terms, but do not have the same ill-conditioning problems of simpler polynomials, such as $f_n(x) = x^n$.

There are a few limitations when using a polynomial series to represent the displacements of the entire wing. First, since the grid is transformed into a unit box, the points must be somewhat uniform on the grid. For instance, if there are 10 points on the root chord, then there should be 10 points on each successive chord. Second, the number of terms in the polynomial series must be equal or greater then the number of structural points. $[A] = [Ws][Ws]^T$ is singular if this condition is not met.

2.9.2 Shape Functions

Shape functions can be used to represent deformations in functional form. (Ref. 10) Deformations of a structural set of points can be interpolated to an aerodynamic set of points. The grid of structural points is first transformed into a rectangular grid as illustrated in figure 4. Each square cell is an isoparametric eight-noded quadrilateral. (Ref. 11) Only nodes that lie on a real spar or rib are of interest. We use the following quadratic interpolation functions on each cell:

$$N_1 = -\frac{1}{4}(1-s)(1-t)(1+s+t)$$

$$N_2 = -\frac{1}{4}(1+s)(1-t)(1-s+t)$$

$$N_3 = -\frac{1}{4}(1+s)(1+t)(1-s-t)$$

$$N_4 = -\frac{1}{4}(1-s)(1+t)(1+s-t)$$

$$N_5 = \frac{1}{2}(1-s^2)(1-t)$$

$$N_6 = \frac{1}{2}(1+s)(1-t^2)$$

$$N_7 = \frac{1}{2}(1-s^2)(1+t)$$

$$N_8 = \frac{1}{2}(1-s)(1-t^2)$$

The coordinates s and t are normalized coordinates for each cell as shown in figure 4. By locating the cell in which an aerodynamic point lies, the displacement of the aerodynamic point can be found when performing the following summation over the structural points of the cell.

$$z_a = \sum_{i=1}^{8} z_i N_i$$

The transformation matrix, D, can be found by cycling through all aerodynamic points.

$$Z_a = D\theta$$

where Z_a and θ are vectors of displacements for the aerodynamic points and the structural points respectively. By the following derivation, the proper transformation for forces is found. Begin by requiring that the work done by forces in the aerodynamic grid, F_a, be equal to the work done by the forces on the structural grid, F_s.

$$F_s^T\theta = F_a^T Z_a$$

$$F_s^T\theta = F_a^T D\theta$$

$$F_s^T = F_a^T D$$

$$F_s = D^T F_a$$

Using this relationship to find equivalent forces on the structural grid results in forces that preserve the conservation of forces and moments.

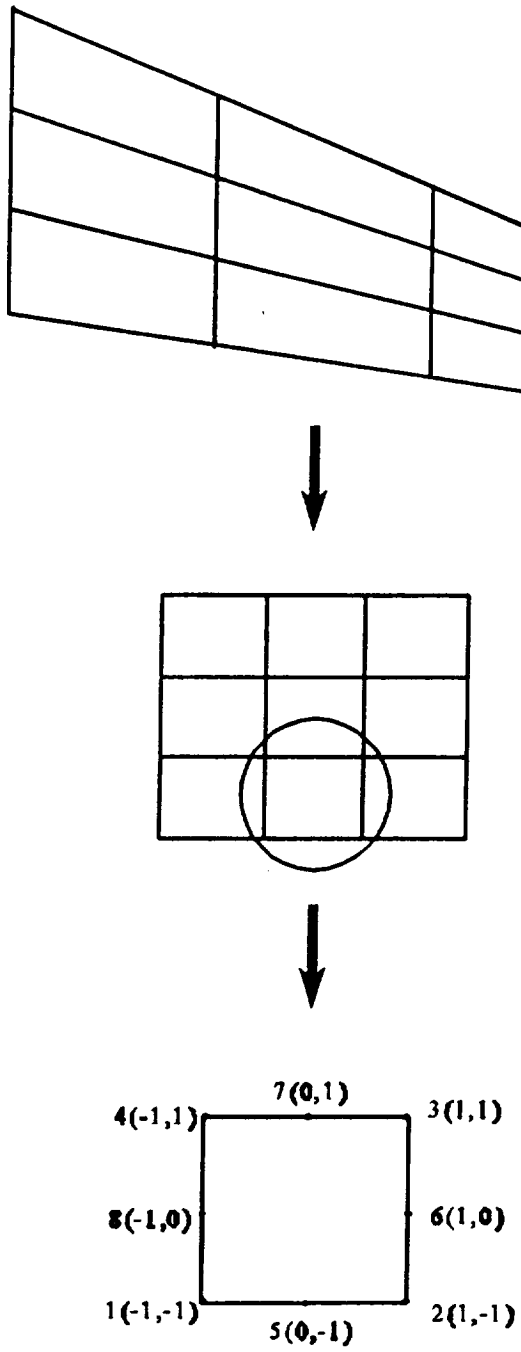

Figure 4. Grid Transformation

CHAPTER 3

WING SHAPE PARAMETERIZATION

3.1 Introduction

This chapter describes how the model is constructed. It is important to model the shape of the wing box as accurately as possible. The wing shape geometry is defined by ACSYNT. The automatic generation of the finite element mesh will be discussed. The internal geometric layout of spars and ribs is also covered in this chapter.

3.2 Wing Segmentation

The wing is segmented into trapezoidal sections to help maintain a more accurate definition of the shape of the wing box. Each section has a constant sweep angle. A change of sweep would lead to a new section. Figure 5 illustrates the segmentation of the planform of a Concorde wing. This allows the planform of each section to be a simple trapezoid which can then be easily divided into triangular membrane elements. Segmenting the wing in this manner allows for great flexibility in new innovative planform designs. Partially swept forward wings can be tested and models for wings, such as the Concorde wing, can be easily and accurately constructed.

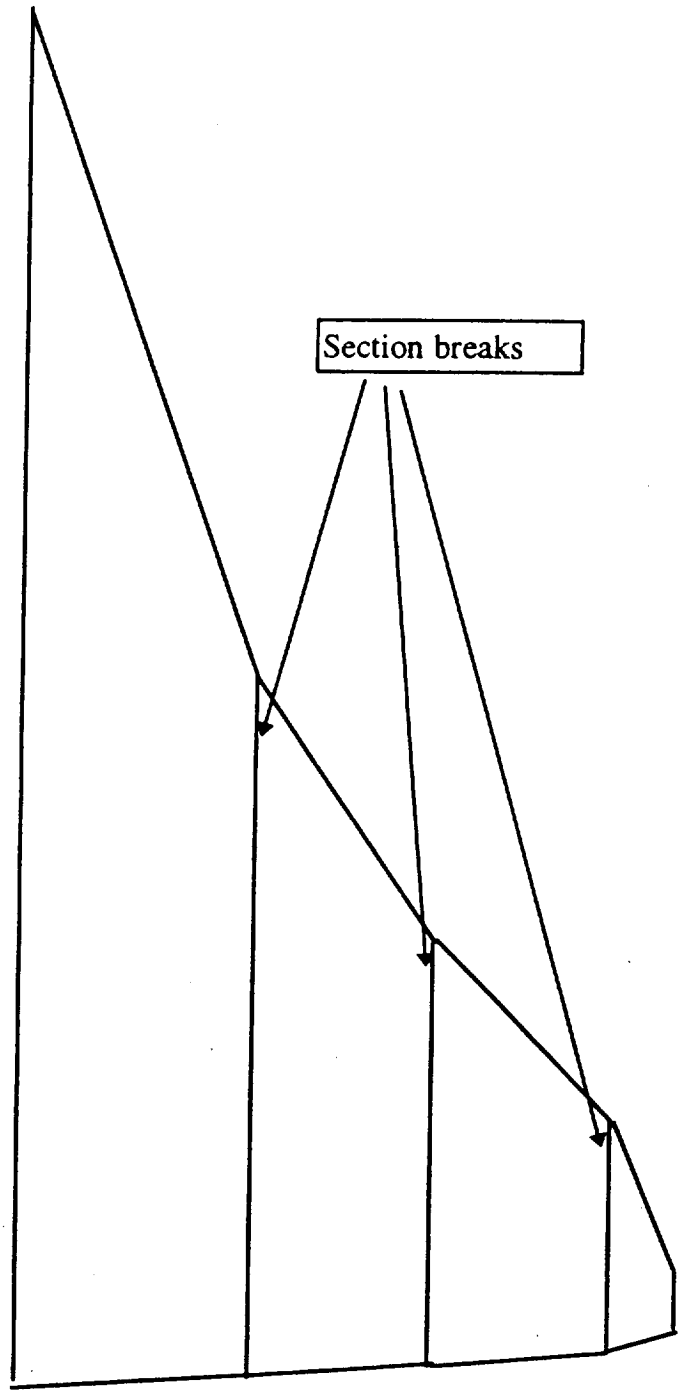

Figure 5. Wing Segmentation

3.3 ACSYNT Geometry Definition

The geometry of the wing is obtained from ACSYNT. Following the same segmentation scheme as previously described, ACSYNT provides airfoil cross-sectional data for each segment. Beginning at the root chord and continuing to the tip chord, cross-sectional data consisting of the airfoil shape is given for each segment. The airfoil shape is defined by xyz coordinates of a point on the airfoil. These points are linearly connected from root to tip of a segment to form the shape of the airfoil. The same number of points are given for each cross-section and the listing of the points always begins at the trailing edge. This creates a one-to-one correspondence of points from one cross-section to the next. These points are connected linearly to form the upper and lower surface of the wing. Figure 6 shows a typical segemented wing geometry. The points on the airfoil that are data points from ACSYNT are shown. Also illustrated in figure 6 is the manner in which CDOSS connects the points to form the wing surfaces. Since the leading edge and trailing edge control surfaces do not provide significant structural strength, we exclude them and only analyze the wing box. The control surface are defined as a percent of the chord. The leading edge and trailing edge spars are placed at the leading edge of a trailing edge flap and at the trailing edge of a leading edge flap, respectively, to connect the upper and lower surface. The wing box is constructed and ready for mesh generation.

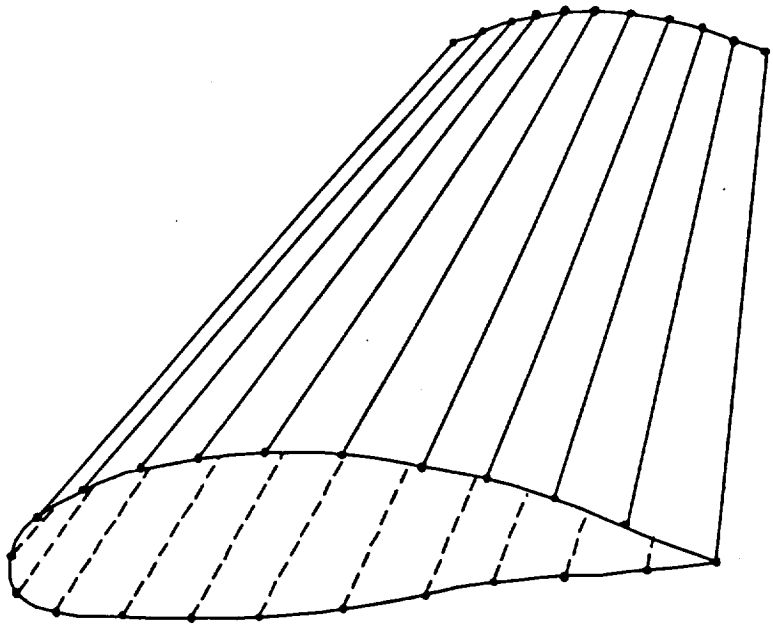

Figure 6. Wing Geometry Using ACSYNT Data

3.4 Automated Finite Element Model Generation

The capability for automated finite element model generation is essential for efficient conceptual design analysis. (Ref. 12) Creating finite element input files by hand is both time-consuming and tedious. CDOSS has the capability to take the geometry given by ACSYNT and create a finite element model. Automatically, all of the nodes, membrane elements and truss elements are created automatically using the following guidelines. Nodal points exist on the upper and lower surface anywhere spars and ribs intersect (including "dummy" spars and ribs). These intersections also define quadrilateral cells on the skins, each with four nodes. These quadrilateral cells are divided into two triangular membrane elements. Webs for all spars and ribs are divided into quadrilateral cells between upper and lower nodes along the spar and rib lines. These quadrilateral cells are also divided into two triangular elements. Truss elements are placed between nodes along spar and rib lines on the upper and lower surface for the real structural elements only. "Dummy" spars and ribs do not have caps. All elements are also assigned thickness or area while generating the elements. Figure 7 illustrates how all of these elements are used to model a wing using the automatic mesh generator. These guidelines make it possible to generate the entire wing model where nodes are defined by geometric coordinates, elements are defined by nodes, and design variables are assigned appropriately.

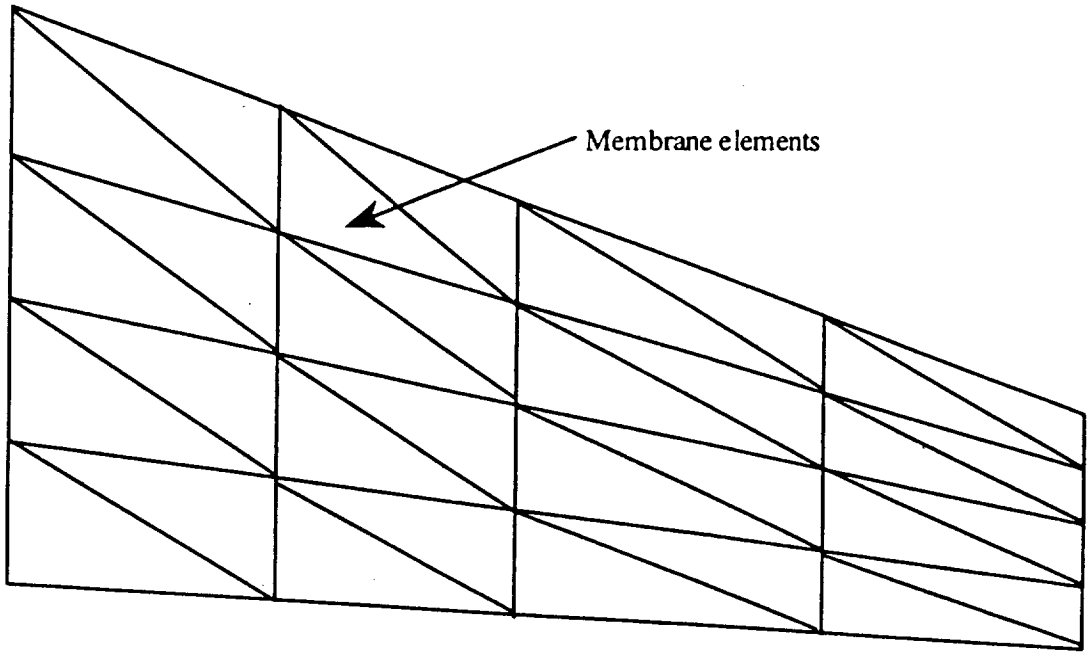

Cover Skin

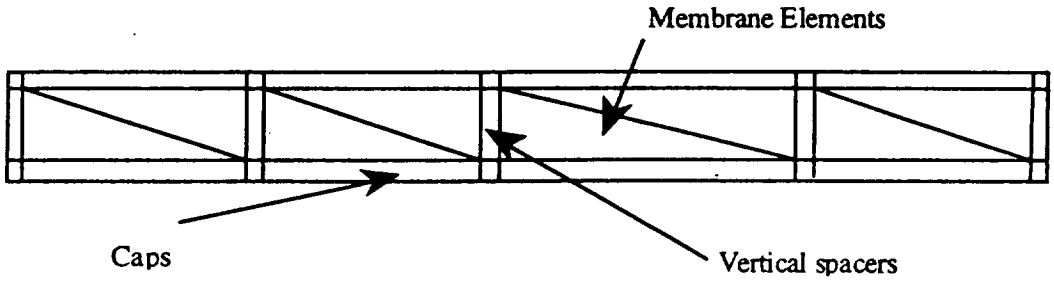

Spar or Rib

Figure 7. Mesh Generator Example

3.5 Layout of Spars and Ribs

For the conceptual design phase, flexibility in the design is important. One aspect of the design is the layout of spars and ribs in the wing box. CDOSS is capable of two different spar configurations. The first option is 'fanned' spars. Spars are spaced evenly at each cross-section and extend from the root to the tip. The spars are continuous with bends at section breaks. The second option is parallel spars. In this configuration, the spars are parallel to the trailing edge of the wing box. The spars are evenly spaced at the root chord and run parallel to the trailing edge of each section. The spars are continuous to the tip unless they intersect the leading edge, where the spar would then end. At each section break, the spar continues but runs parallel to the trailing edge of the next section. Figure 8 illustrates both of these configurations. In both spar configurations, the number of spars beginning at the root is a design variable. "Dummy" spars are added between real spars to refine the mesh and follow the same configuration guidelines as real spars.

The layout of ribs depends on the choice of spar configuration. CDOSS is presently limited to ribs parallel to the root rib. The number of ribs is a design variable. Each section can have a different number of ribs. For fanned spars, the ribs are spaced evenly between section breaks and "dummy" ribs are added between real ribs to refine the mesh. For parallel spars, ribs are placed at points in which a spar intersects the leading edge. This is necessary to ensure that quadrilateral cells are created for finite element model generation. If additional ribs are desired, they are placed between

existing ribs. These options for spar and rib configuration offer some flexibility in conceptual wing design.

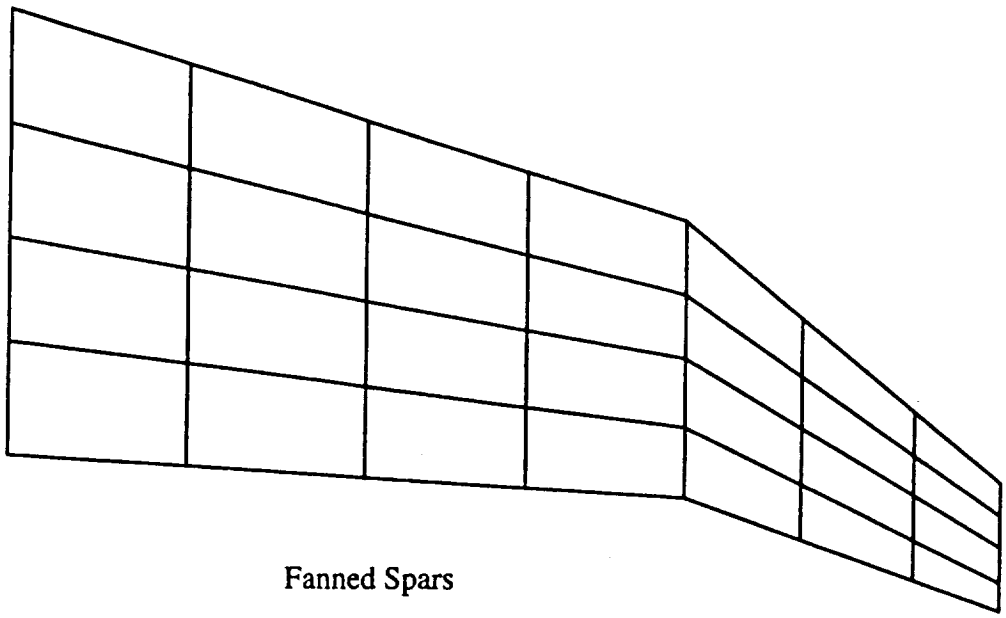

Fanned Spars

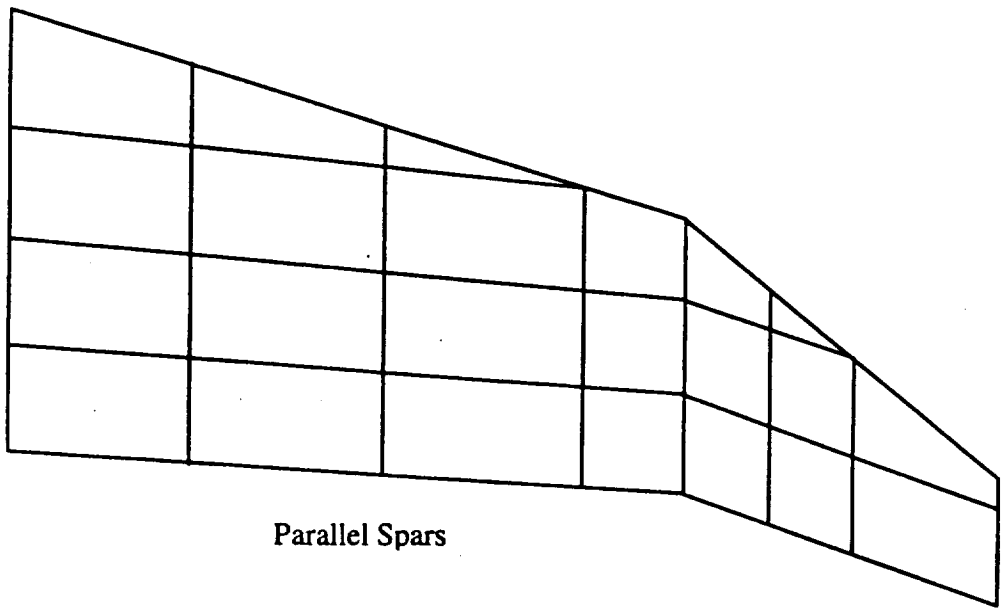

Parallel Spars

Figure 8. Spar Configuration

CHAPTER 4

BEHAVIOR CONSTRAINTS

4.1 Introduction

Behavior constraints are the key to optimization. The constraints represent design limitations and failure modes. Deformation constraints may represent stiffness requirements. Stress constraints protect against failure in yield or fatigue. We use a simple comparison of the stress in an element to the maximum yield stress, taking into account the margin of safety. Buckling constraints are very critical for wings. As the wing bends up in flight, the upper surface experiences large compressive stresses. Behavior constraints are discussed in detail in this chapter.

4.2 Deformation Constraints

4.2.1 Boundary Conditions

Wing deformations are constrained as follows. The root chord is fixed to a reference surface. All degrees of freedom are not allowed to move at the root chord. The rotational degrees of freedom are fixed throughout the wing. This is because of the use of CST and truss elements which cannot resist local rotation at their nodes.

4.2.2 Behavior Constraints

Constraints on the amount of deformation at the nodes or deformations of the elements in relation to each other could also be constrained.

4.3 Stress Constraints

Each element is associated with a behavior constraint on stress. The material has a given yield strength that each element cannot violate. The truss elements have a single, scalar axial stress. The axial stress multiplied by the margin of safety cannot be greater than the yield strength. We have assumed that compressive yield strength is the same as tensile yield strength. Membrane elements have two in-plane stresses and a shear stress. We use an equivalent Von Mises stress for comparison with the maximum yield stress.

$$\text{Equivalent Stress} = \text{sqrt}(\sigma_1^2 - \sigma_1\sigma_2 + \sigma_2^2)$$

where σ_1 and σ_2 are principle stresses. The equivalent stress multiplied by the margin of safety cannot be greater than the yield strength.

4.4 Buckling Constraints

Panel buckling constraints are very important in the optimization routine of airplane wings. In most cases, the buckling constraint is the determining factor for changes in the design variable for the wing skin. In order to perform a buckling analysis, the panels must first be identified and panel stresses calculated. Then, buckling constraints can be evaluated.

4.4.1 Panel Identification

Panels must be defined by the real structure where there is rib or spar support. Intersection of real spars and ribs serve as supports for the panels on the wing skins and in the spar and rib webs. By defining the panels this way, each panel has many triangular membrane elements within it. In figure 9, the section of the wing skin shown has three real spars, two "dummy" spars, three real ribs, and three "dummy" ribs. This section has four buckling panels. Each panel has eight triangular membrane elements. The dummy elements do not provide support for the buckling panels. Each panel is identified by the nodes at the four vertices and the membranes that make up the panel. The average of the thickness of the membranes in a panel is used as the panel thickness. Using the coordinates of the four vertices, the edge lengths are calculated. The panel dimensions are the average of the two lengths in each direction. Thus, each trapezoid panel is approximated as a rectangular panel. Membrane normal and shear stresses are

averaged to obtain the panel normal and shear stresses. These dimensions and stresses are found for each panel, so that simplified buckling analysis can be performed on each panel.

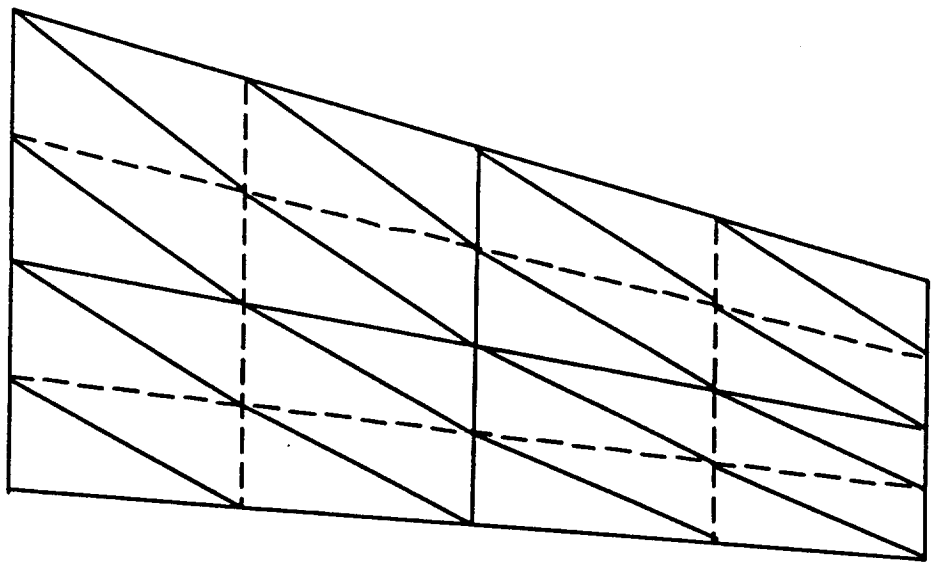

Figure 9. Panel Identification

4.4.2 Buckling Analysis

A simple conservative approach was adopted for the buckling analysis. We assume each panel to have simply supported edges. Actually, there is always more rotational stiffness along panel edges. This simplified buckling analysis used ratios of the panel stresses to the critical buckling stresses. Stresses are rotated to local stresses since the rectangular panel is oriented in local coordinates. Figure 10 illustrates the approximation of the trapezoidal panel as a rectangular panel. The local stresses used to perform the buckling analysis are also shown. Critical buckling stresses are functions of material properties and panel dimensions. (Ref. 13-15) A simple interaction equation was used for the constraint. Since the normal stresses and shear stresses all affect one another, we cannot perform the buckling analysis for each stress individually. The buckling interaction equation is as follows (Ref. 17):

$$g = 1 - \frac{N_x}{N_{xcr}} - \frac{N_y}{N_{ycr}} - \left(\frac{N_{xy}}{N_{xycr}}\right)^2$$

Critical buckling stresses are negative. Compressive panel stresses are also negative. If g, the constraint value, is negative, then the panel will buckle. This procedure is carried out for each panel to check for buckling. Another approach to buckling analysis is a global approach where constraints are based on a linear eigenvalue analysis of the entire structure. (Ref. 18) The advantage of this approach is that it allows interaction of the individual panels. The disadvantage is additional computation time is needed to solve an eigenvalue problem. The simplified local panel buckling analysis used in CDOSS is

much faster. Also, this approach is easily applied to composites by simply modifying the equations for panel stresses and critical stresses. (Ref. 19)

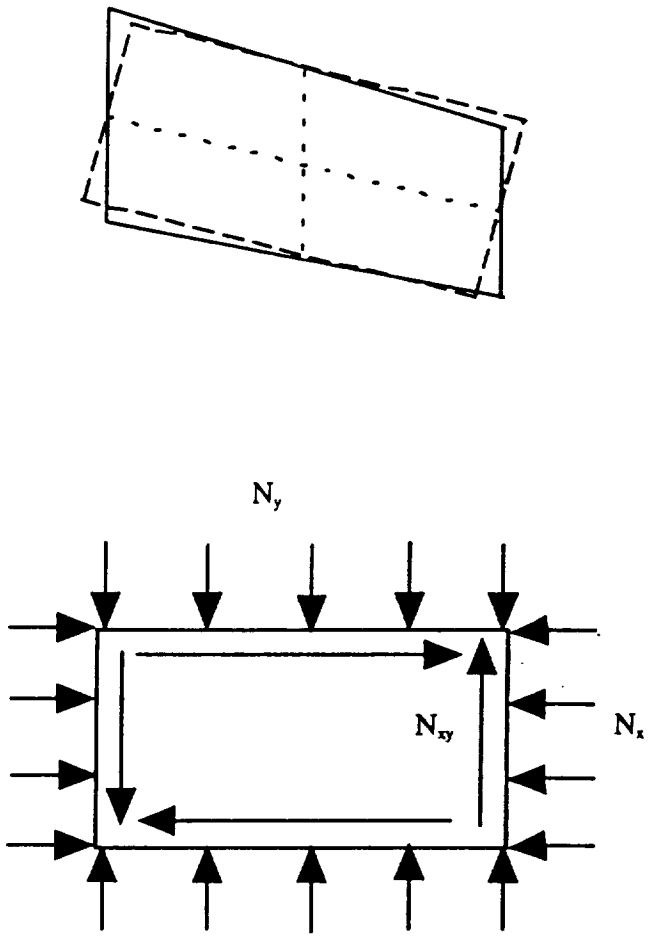

Figure 10. Panel Approximation

CHAPTER 5

STRUCTURAL WEIGHT EVALUATION AND OPTIMIZATION

5.1 Introduction

It is very difficult to obtain accurate wing weight for the conceptual design phase. Details, which are not a part of conceptual design, account for a considerable portion of the weight. Such details are fittings, joints, attachments, and access doors, for example. There are different methods of estimating structural weight which will be discussed in the chapter. We will also cover the optimization algorithms used. CDOSS uses a simple optimality criterion, although there are more rigorous nonlinear optimization techniques which require more computation time. (Ref. 20-25) In this chapter, we will discuss the technique used in CDOSS.

5.2 Weight Evaluation

Several different methods of weight estimation have been used in conceptual design. One method is statistical weight estimation. (Ref. 1) This method is dependent on a database of existing airplane designs. Statistical weight estimation does not give accurate results for non-conventional airplane designs and does not take into consideration more detailed design variations such as chord extensions or varied wing thickness distribution. (Ref. 26) Another method is a theoretical estimate of bending

weight. (Ref. 26) Many constraints are accounted for using this method, such as bending stress, buckling and local pressure loads. A more structurally efficient design can be achieved. The disadvantage of bending weight estimates is that the results are less accurate as particular considerations, such as buckling, dominate the sizing of the structure. (Ref. 26)

CDOSS uses a method that is more accurate than statistical estimates, simpler than bending weight, and takes advantage of the data calculated in the finite element analysis and optimization. All of the major structural elements are identified for the finite element model. All of the elements of the finite element model are sized within the optimization routine. To obtain the structural weight of an airplane wing, we simply calculate the volume of each element, sum the volumes, and multiply by the density of the material. This method results in fairly accurate structural weight estimates for conceptual designs using little computing time. Any approximations in modeling the structure will change the final weight estimate. Statistical, empirical correction factors used to convert the idealized weights of skins, caps and webs to real weights taking manufacturing techniques into account. The structural weight estimating technique used in CDOSS is an efficient method for preliminary design.

5.3 Structural Optimization

Automated multidisciplinary optimization is necessary to numerically handle many competing design constraints. (Ref. 27) While rigorous mathematical programming techniques are established for structural synthesis (Ref. 24), the method used in this work is an optimality criterion method using fully-stressed design and buckling constraints for structural optimization. This is done mainly for the sake of simplicity at this stage. (Ref. 29)

5.3.1 Element Sizing

This is the approach used in CDOSS. A fully-stressed design is based on stress constraints. Each individual element is sized based on a ratio of element stress to maximum yield stress. (Ref. 29) The thickness or area of the element is increased or decreased based on the ratio of the element stress multiplied by a safety factor and of the maximum yield. The new size is the ratio multiplied by the present size. Since strength is a linear function of thickness stress (assuming internal forces do not change much from iteration to iteration), this method is effective. Analytic sizing for buckling is much more difficult. Buckling stresses are cubic functions of thickness. Within the constraint equation, the in-plane normal stresses are not of the same order as the shear stress. (Ref. 21,24) For these reasons, the sizing for buckling is based on a pre-selected value of the buckling constraint. The decision of whether to increase or decrease the

thickness of the panel is dependent on the value of the constraint function. If the constraint value is negative, the panel is buckling and the thickness should be increased. If the constraint value is positive, then the thickness should be decreased. The sizing for buckling iterates until all panels have a constraint value between zero and one tenth.

5.3.2 Optimization Routine

The optimization routine calculates the new thickness for stress and buckling constraints separately, then compares them. The new thickness or area does have maximum and minimum limits that are determined from other constraints, such as manufacturing constraints. The new thickness from the stress and buckling constraints are compared to the minimum limit. The largest of these three values is compared to the maximum limit. The smallest of these two values is the new thickness assigned to the element. This optimization routine will iterate until the solution converges. Following each iteration, stresses and weight are calculated based on the new values for thickness. The convergence check first requires that no stress constraint is violated by more than 5%. The second requirement for convergence is that the percent change in weight between the present weight and the weight of the previous iteration is not more than a selected tolerance criteria. The method of optimization is effective in ensuring that both stress and buckling constraints are not violated. Since the calculations are simple, this optimization routine is also very efficient.

CHAPTER 6

TEST CASE: FIGHTER TYPE WING

6.1 Introduction

The test case used for this work was a typical fighter all aluminum wing. This chapter discusses the modeling of the wing and the load cases used. An analysis of the load results will also be covered in this chapter. Optimization and weight results will also be discussed. All measurements are in English units (inches, pounds, etc.).

6.2 CDOSS Wing Model

The CDOSS fighter wing model very closely resembles an actual wing. The CDOSS model is a model generated from ACSYNT cross-section data using the design options available in CDOSS. The table 1 shows a comparison of major features of the CDOSS model and an industry quality finite element model.

Table 1. Comparison of CDOSS and Industry Models

Feature	CDOSS Model	Industry Model
Number of Spars	12	11
Number of Ribs	5	5
Length of Root Chord	85	80
Length of Tip Chord	20	10
Half Span	140	130

The spar and rib layout match nearly exactly with spars parallel to the trailing edge and ribs parallel to the root chord. The dimensions are only slightly different. The CDOSS model is a little larger than the actual wing box. Figures 11 and 12 show the finite element meshes for the CDOSS model and the industry model. No "dummy" spars were used for the CDOSS model of the wing. There are five "dummy" ribs, represented as dotted lines in figure 11. There are a few other minor differences in the finite element meshes, such as more structure and more detailed mesh on the industry model where pylons or external stores would be supported. Also, the industry mesh used quadrilateral elements rather than triangular elements. CDOSS automatically generated a very accurate model of the fighter wing box.

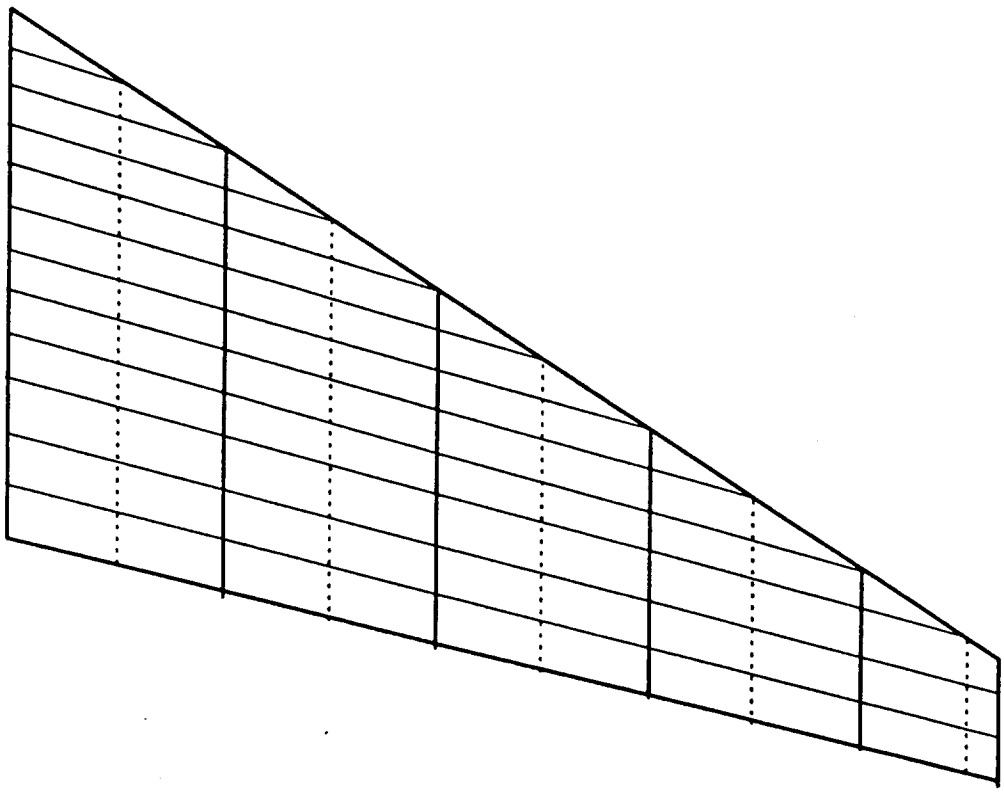

Figure 11. CDOSS Wing Mesh

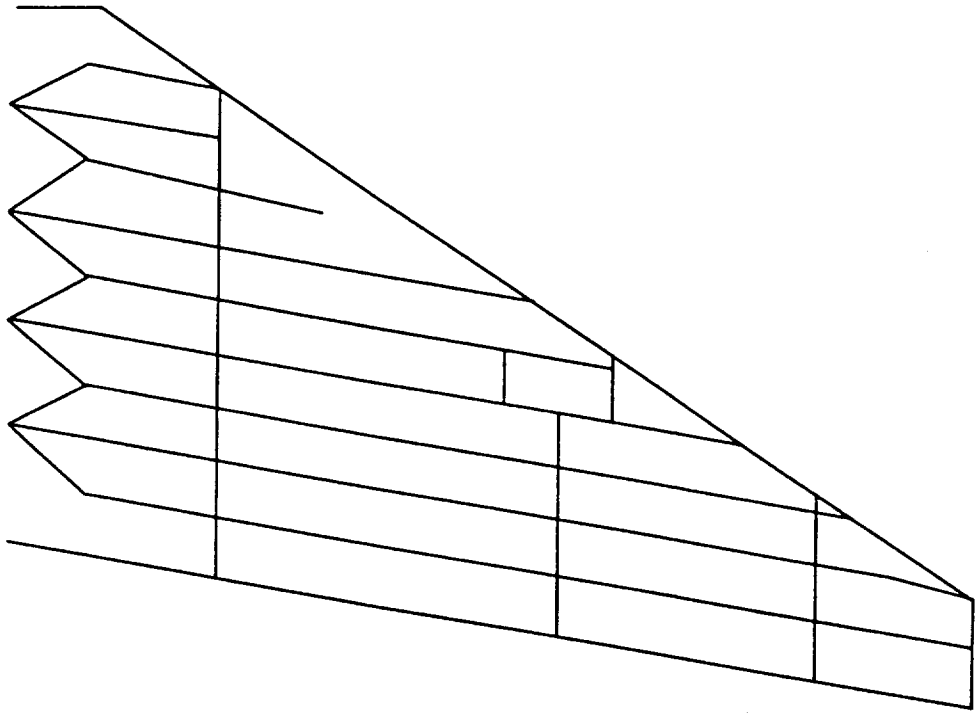

Figure 12. Industry Finite Element Wing Mesh

6.3 Load Cases

Two load cases were analyzed for the fighter wing. The first load case was a simple 1000 pound point load applied to the rear spar at the tip. The second load case was a 9 'g' pullup at .9 mach, 10,000 feet altitude, 21,289 pounds gross weight, and tip missiles. Load data was given as concentrated loads at the nodes of the industry mesh. These loads were interpolated to the nodes of the CDOSS mesh. Since there are no "dummy" spars, there are no "floating" nodes. Thus, every node on the mesh is supported by real structure and can carry loads. Since the meshes are so closely matched, the interpolation was very simple. The tip load is a simple load case that is not representative of realistic loads on a fighter. It is possible to use this load to predict the displacements and reaction of the model and to assess convergence characteristics and effects of various constraints. Also, empirical data was available for the industry model and from an Automated Structural Optimization System(ASTROS). (ASTROS is being developed by the U.S. Air Force.) The ASTROS model has the same mesh as the industry model. The 9 'g' load is a typical maneuver of a fighter airplane. This load case models one of the critical maneuvers which the airplane is designed to perform.

6.3.1 Comparison of Transformation Methods

In the case of the aerodynamics loads, forces must be transformed to the structural grid. The two methods described in chapter 2 used functions to represent the deformations. The shape function method was applied to individual cells. The Chebychev polynomial method was applied to the entire wing. Since the Chebychev method requires that the structural grid be uniform, a different model was used for this comparison. The model is illustrated in figure 13. There are 5 real spars and 6 'dummy' spars between the leading and trailing edge spars. Spars are fanned and run from root to tip. There are 3 real ribs and 4 'dummy' ribs between the root and the tip. The most significant difference between this model and the fighter model used in this chapter is that the buckling panels are much larger in this comparison model. The comparison was performed using the 9 'g' load case. In figure 14, the change of the weight per iteration is shown. Figure 15 and 16 show the wing deformation and wing skin thickness along a center spar line after optimization. This comparison shows that the two methods produce very similar results.

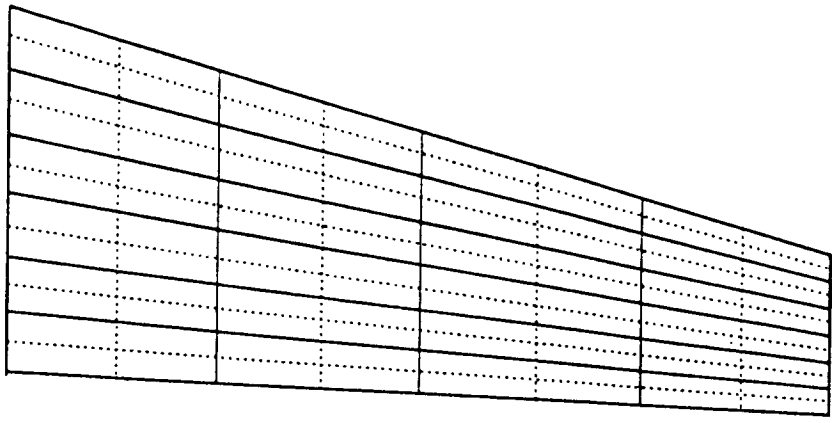

Figure 13. Layout of Comparison Model

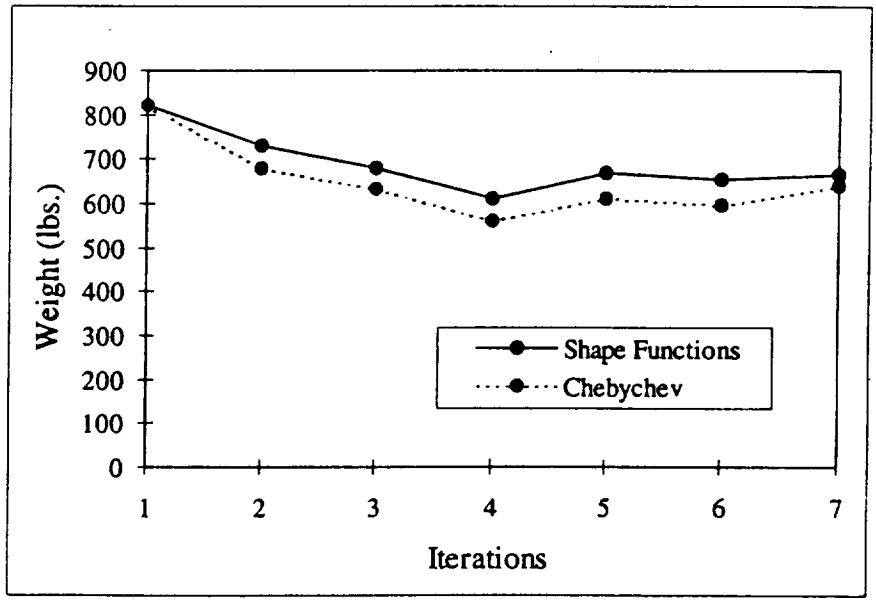

Figure 14. Comparison of Iterations vs. Weight

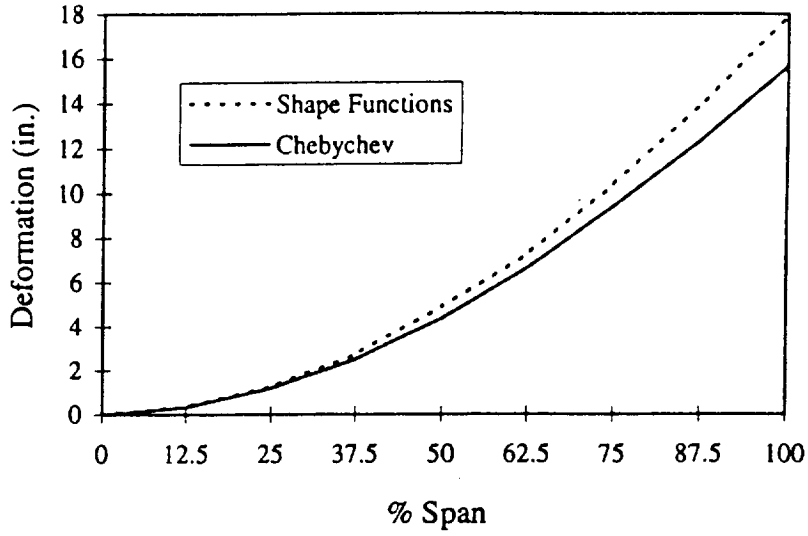

Figure 15. Comparison of Deformations

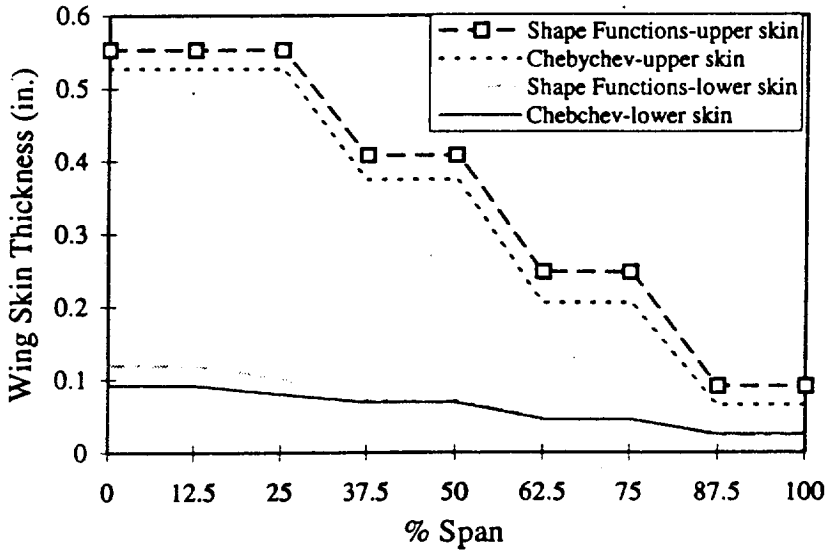

Figure 16. Comparison of Wing Skin Thickness

6.4 Analysis of Results

The analysis of the CDOSS model included deformation analysis and stress analysis. The deformations of each nodal point is given as well as the stress in each element. Deformations can be used to check the flexibility of the structure. The stresses can be compared to the yield stress for each element. This information indicates whether or not the design is feasible. The deformations and stresses to be discussed are results following optimization.

6.4.1 Deformations

The deformations resulting from both the 1000 pound tip load at the rear spar and the 9 'g' load were analyzed. A 1000 pound tip load caused a tip deflection of approximately 1.1 inches. This is fairly close to the 1.3 inch tip deflection of the industry model and the 1.01 inch tip deflection of the ASTROS model. Figure 17 shows a comparison of the deformations from these three models. These displacements are along the rear spar. The CDOSS model is less flexible. There is less bending in the spar compared to the other models. This could be caused by the differences in spar web thickness and spar cap areas. The industry and ASTROS models have spar webs and caps with different thickness and area, respectively. CDOSS (to simplify for conceptual design) averages these values and gives all spar webs and caps the same averaged thickness or area. This will effect the reaction of the structure slightly. The 9 'g' load

case also resulted in feasible results. See figure 18. The 8 to 9 inch deflections at the tip are quite reasonable and are comparable to the results of the ASTROS model. The analysis of the deformations of the CDOSS model showed that the model is successful in representing the fighter wing.

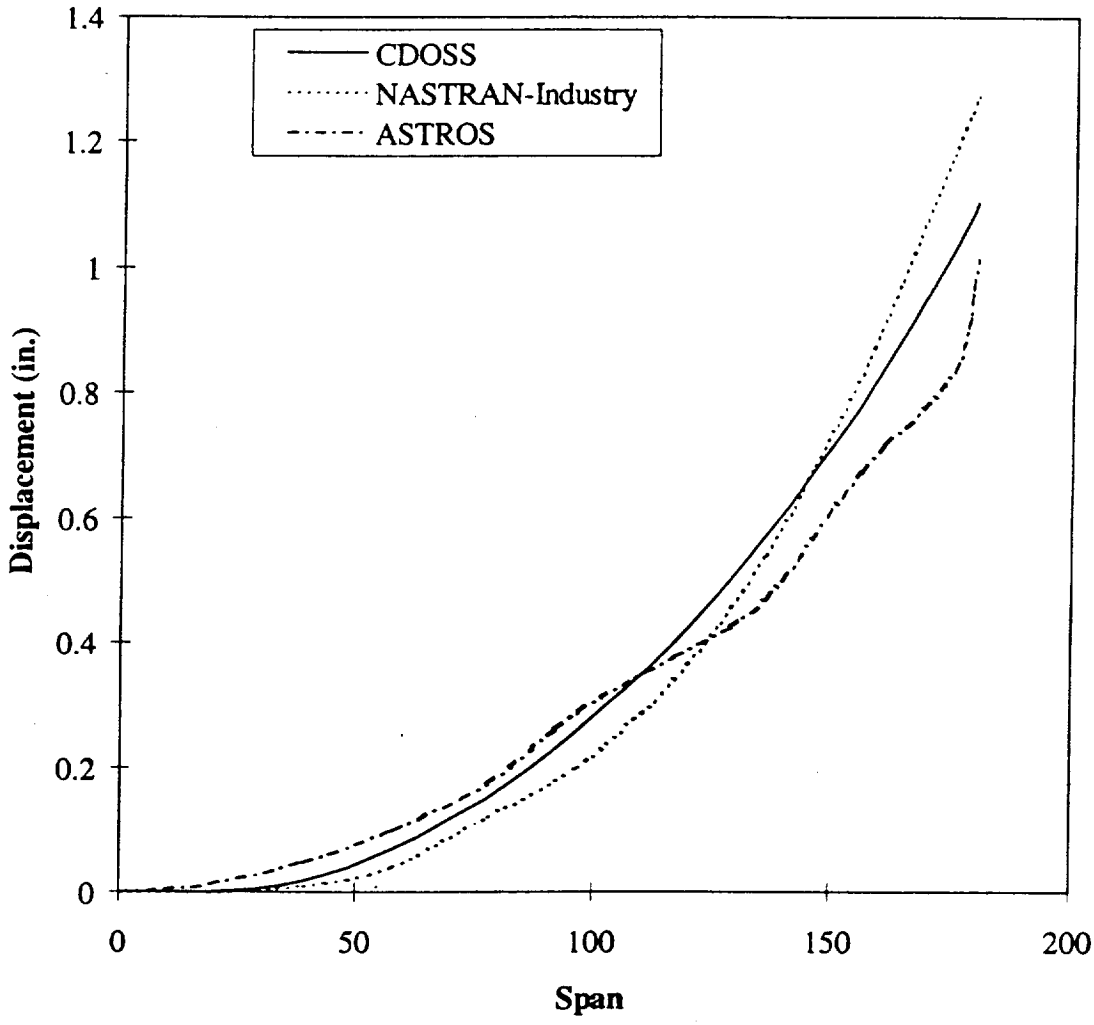

Figure 17. Deformation Under 1000 lb. Tip Load

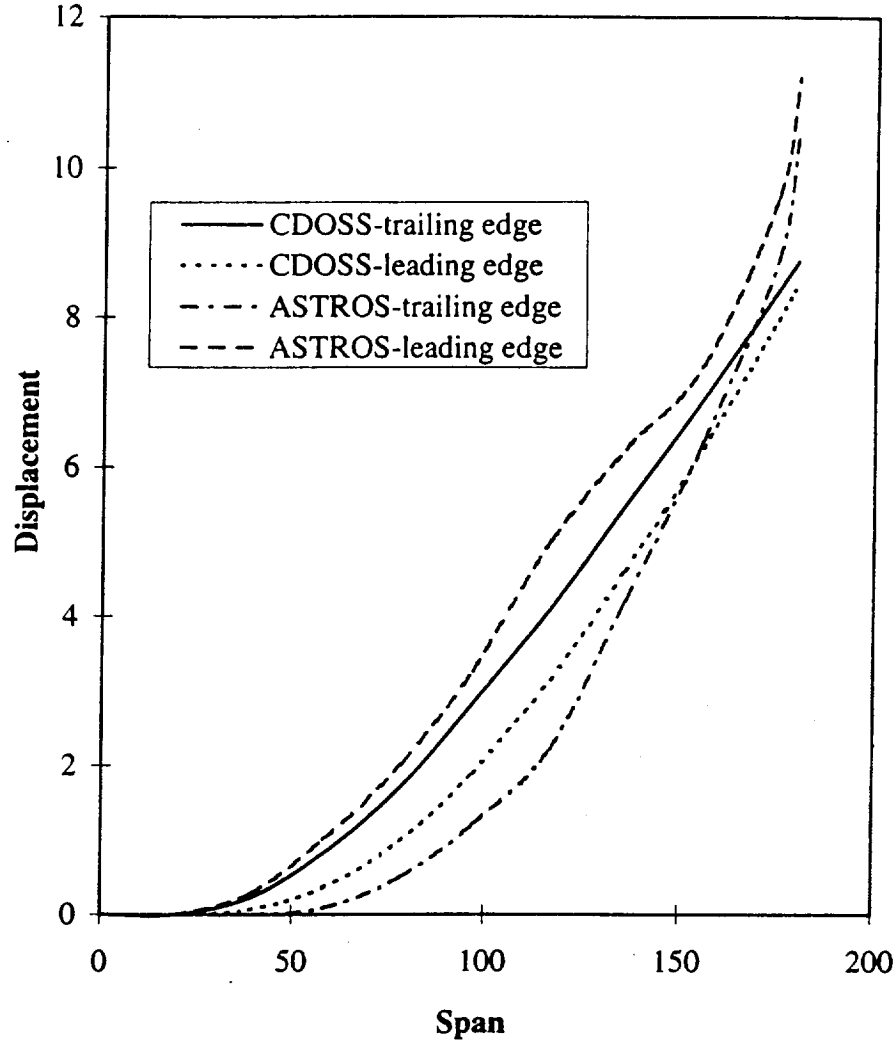

Figure 18. Deformation Under 9 'g' Load

6.4.2 Stresses

The analysis of stresses for both the 1000 pound tip load and the 9 'g' load were performed. Figures 19 and 20 show that neither load case was close to the yield stress. The stresses plotted are taken at the mid-chord line along the span. For the tip load, the absolute values of normal stresses were below 2000 psi and the absolute values of shear stresses were below 4000 psi. These low values show that the tip load is not a critical load when designing this wing. The plots are fairly symmetric. When either the upper or lower surface is in tension at a particular point along the span, the other surface is in compression. The values of tension and compression are comparable and tend to increase from root to tip. The 9 'g' load case resulted in much higher values of stress than the tip load. The stress was as high as 35,600 psi at one point. The value is far from the yield stress of aluminum (60,000 psi) and several 1000 psi less than the margin of safety yield stress (43,000 psi for a 1.5 margin of safety). As expected, when one surface is in tension, the other is in compression as the same point along the span. The values are not nearly as symmetric as they were for the tip load. The values tend to decrease from root to tip. By analyzing the stress distribution, it is possible to identify which sections of the wing may need extra material.

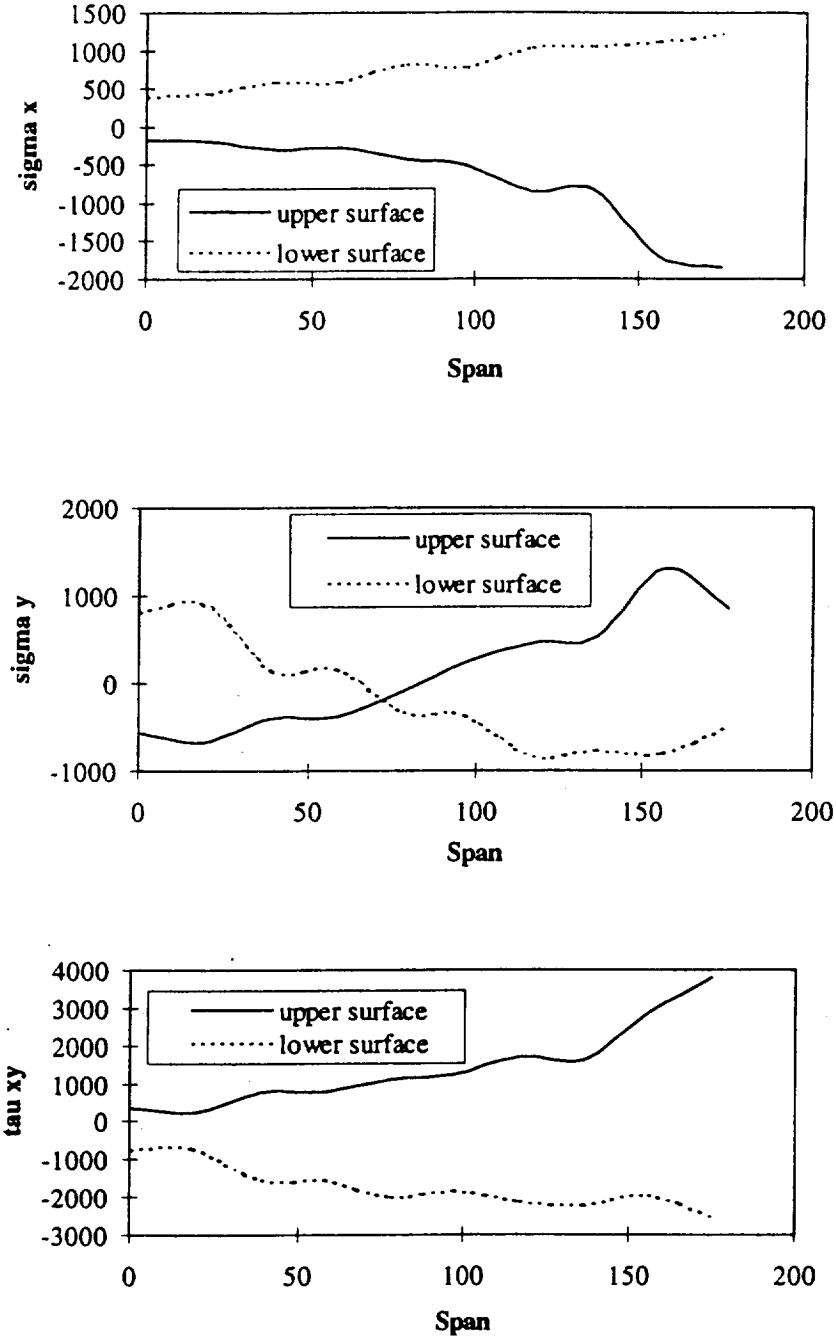

Figure 19. Stresses for 1000 lb. Tip Load

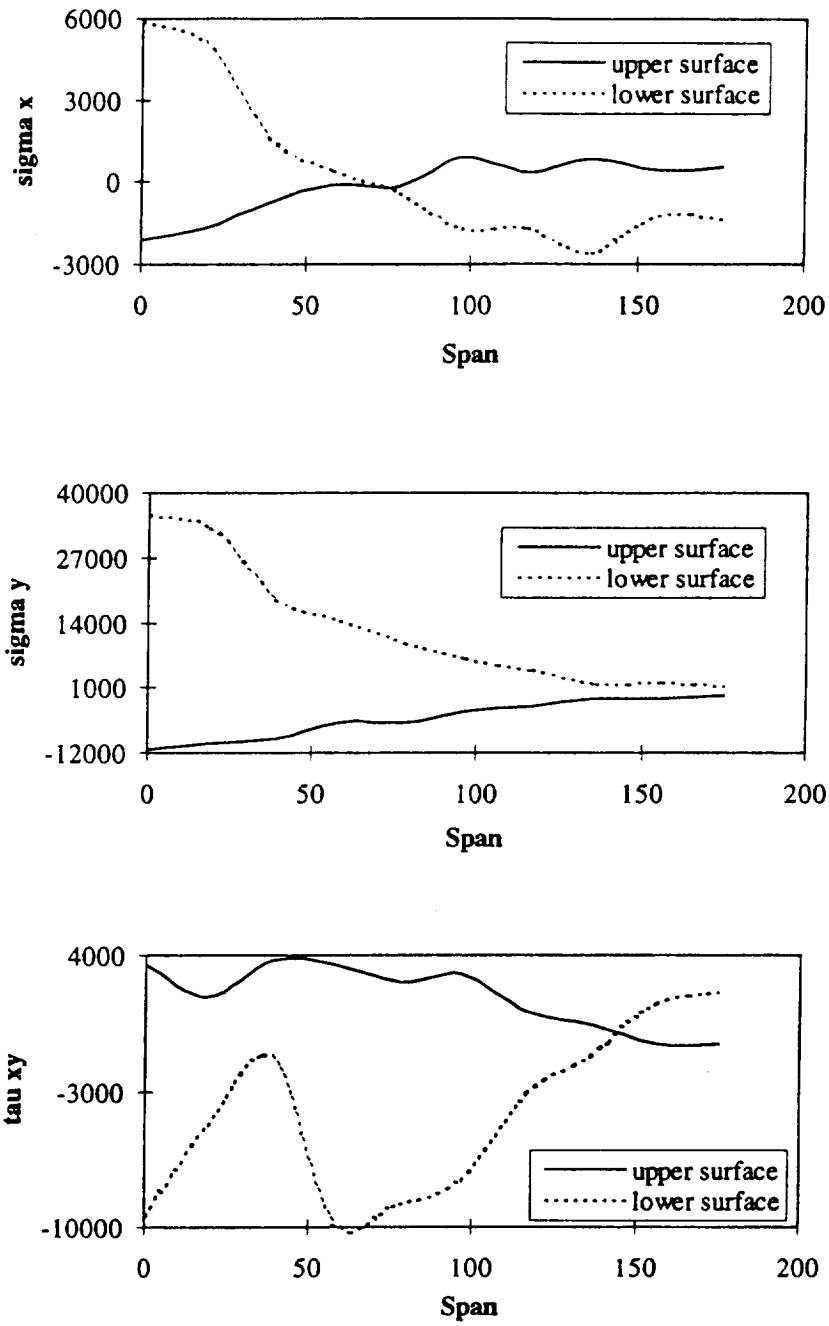

Figure 20. Stresses for 9 'g' Load

6.5 Optimization Results

The optimization routine optimizes the wingskin thickness under deformation, stress, and buckling constraints. The results of the optimization were wingskins thinner than the actual fighter wingskin. Figure 21 shows a comparison of the thickness of the wingskin at the mid-chord line along the span. The 1000 pound tip load case produced extremely thin skins. This result is not surprising because this load case does not represent a realistic loading. Since the loading did not produce a great deal of stress in the structure, as was seen in the previous section. The buckling constraint was the determining factor for the thickness. Without the buckling constraint, the skin would have reduced to the minimum gage allowed without violating any stress constraints. This is also true for the 9 'g' load case. (Minimum gage in these test cases was .005 inches.) The wingskin thickness more closely resembled the actual wing for the 9 'g' load because this a more critical load case. The lower surface is mostly in tension so the buckling constraint is not as dominant in the skin sizing. Figure 21 shows that the real skin thickness is much greater than thickness of the 9 g loading for the real wing. Many other considerations such as numerous other aircraft maneuvers, flutter, fatigue, internal pressure, external loads (engines, stores), etc. must be taken into account. Also, manufacturing constraints probably have a dominate role in the choice of the minimum gage This sizes parts of the wing that have little stress. Thus, the comparisons presented here are only for the sake of assessing global characteristics and computational efficiency of CDOSS.

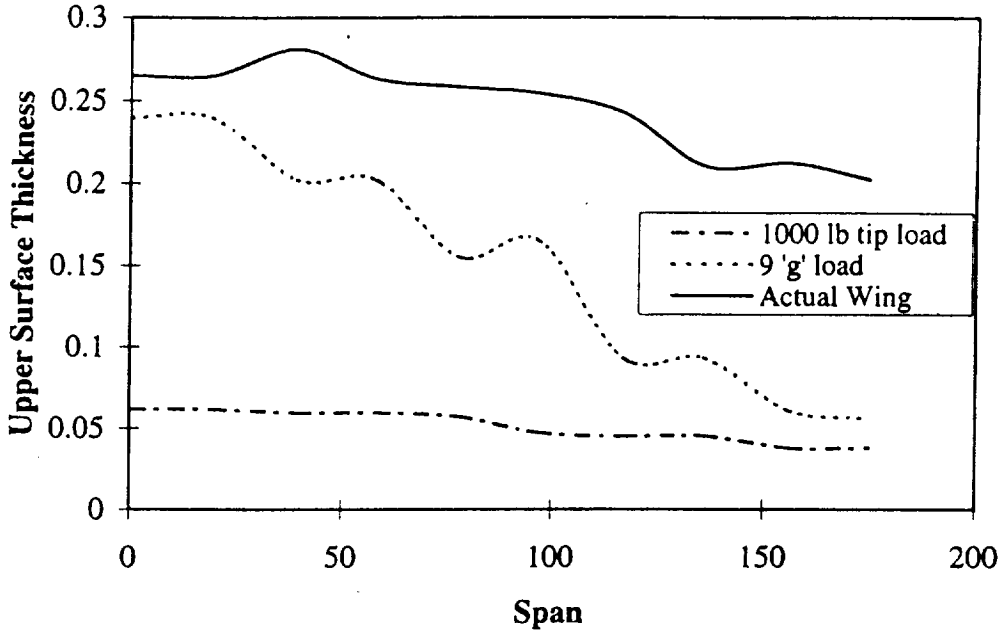

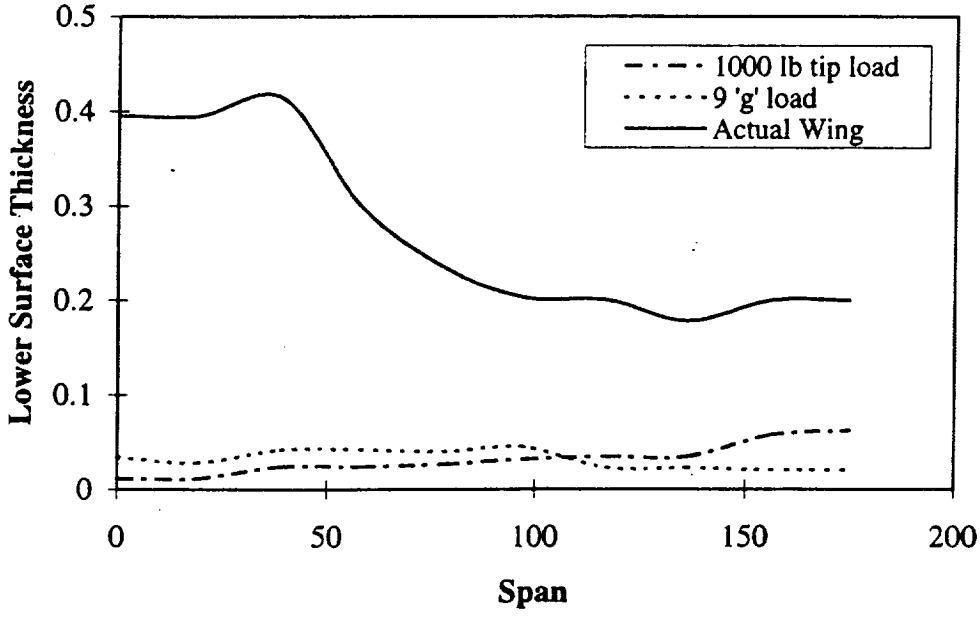

Figure 21. Wing Thickness Comparison

6.6 Weight Results

CDOSS calculates the weight of the wing after each analysis. When optimizing, the weight is calculated after each iteration. Figure 22 shows the change in the weight of the fighter model as the analysis iterates until it converges. The final weight resulting from the tip load is much lower than the final weight from the 9 'g' load case. This is the expected outcome since the tip load is not a realistic load for a fighter. The final optimized weight of the fighter model under a 9 'g' load is 416 pounds. This is a very accurate estimate of the structural weight of the real fighter wing compared to 411.36 pounds calculated from the ASTROS model. It should be noted that no data was available as to exactly what allowables were used in the industry model. Thus, several yield stresses were tried. Figure 23 shows that the sensitivity is fairly high at the lower values of yield stress. Weight is much less sensitive at higher yield stresses. The yield stress of aluminum alloys is approximately 60,000 psi. A material with the same density, but lower yield strength would result in a large increase in weight. The weight results for the fighter test case are excellent estimates of the real wing, thus other designs tested using CDOSS will also result in good estimates of structural wing weight.

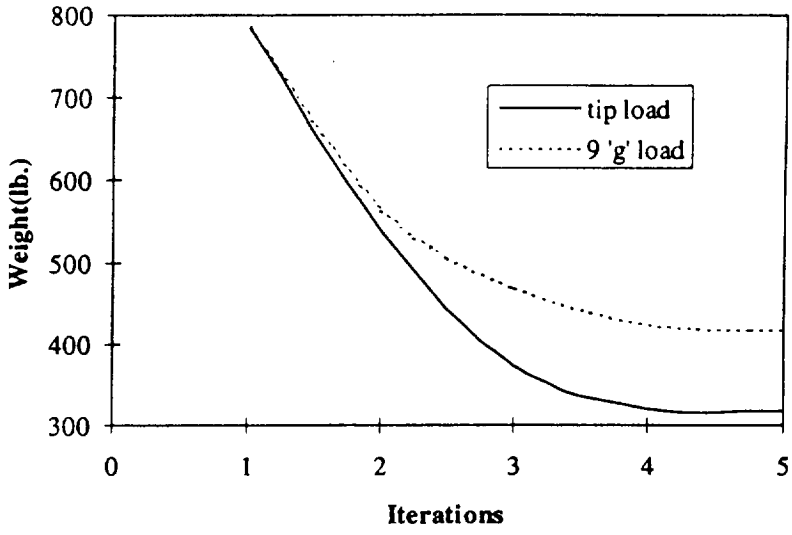

Figure 22. Iterations vs. Weight

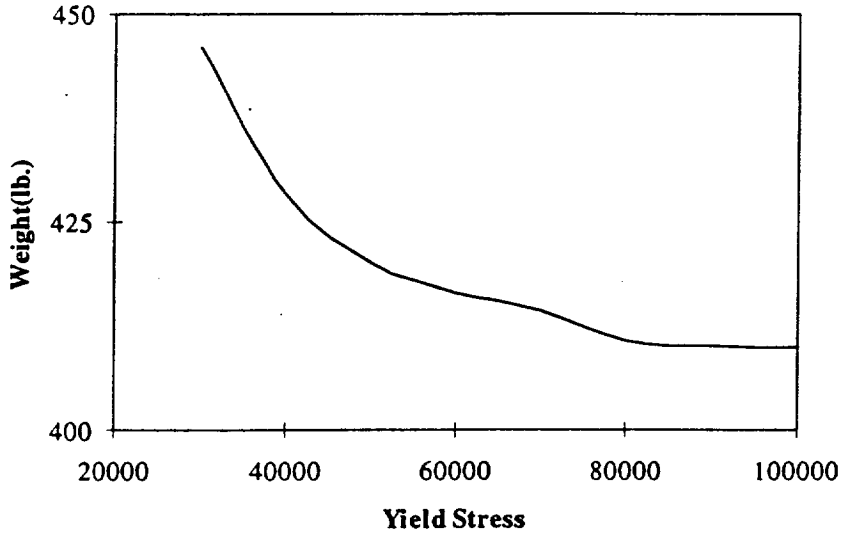

Figure 23. Yield Stress vs. Weight

6.7 Computation Time

CDOSS performs the structural analysis and optimization very quickly. The test cases for the fighter wing required only 33.6 seconds of cpu time to create a mesh, identify panels, and perform 5 iterations of stress analysis and optimization. (These test cases were run on an HP Apollo 700 UNIX based workstation.) Table 2 shows the breakdown of computation time for various steps of the analysis. Creating the finite element mesh and identifying the panels require very little time. Creating the stiffness matrix requires almost 1.5 seconds. The stress analysis requires 7.3 seconds. This includes calculation of deformations, matrix inversion using a LU decomposition technique, stress calculations, and a great deal of matrix manipulation. To perform one iteration of stress analysis and optimization requires almost the same amount of time as a stress analysis alone. Thus the optimization portion is extremely fast. (These time estimates are dependent on the size of the mesh.) Being able to perform the structural analysis in such a short amount of time allows designers to test many designs and modification quickly and efficiently.

Table 2. Breakdown of Computation Time

Step in Analysis	CPU time (sec.)
Get data from ACSYNT & Create Mesh	.1
Panel Identification	.1
Compute Stiffness Matrix	1.4
Perform Stress Analysis	7.3
Perform One Optimization Sequence and a Stress Analysis	7.4

CHAPTER 7

CONCLUSION

The conceptual design oriented structural synthesis capability discussed in this thesis is tailored towards conceptual design. The analysis is accomplished efficiently and the results show good accuracy. The automated mesh generator quickly creates a finite element model for analysis using membranes elements, truss elements, and "dummy" elements. The simple elements allow for easy calculation, manipulation, and sensitivity analysis. The wing modeling is done using airfoil cross-sectional data, wing segmentation, and options in spar configuration. The behavior constraints used were effective for optimization. There are constraints on deformations, stresses, and buckling. Buckling is very important in the sizing of the wing skins. Using a simple interaction equation and averaging the stresses over panels led to simple buckling constraint values that could be used for optimization.

Optimality criterion using full-stressed design and buckling constraints was found to be very efficient and produced adequate results for conceptual design. The weight evaluation is based on the finite element model corrected for manufacturing detail. The test case of a fighter wing showed that CDOSS modeled the wing very well and performed the structural analysis and optimization effectively. The results were compared to other models and to the actual wing. The deformations and stressed were analyzed. The optimization of the wing skins led to reliable weight results.

Computation times are extremely fast. The test case showed that the structural analysis and optimization of a wing in conceptual design can be cost effective and reliable.

This work can also be extended to modeling and analyzing of an entire airplane. Other possible extensions for this work are in the areas of composite materials and added aeroelastic constraints.

REFERENCES

1. Daniel P. Raymer, Aircraft Design: A Conceptual Approach, AIAA, Inc., 1992.

2. Vanderplaats, Garret N., "Automated Optimization Techniques for Aircraft synthesis", AIAA 76-909, in AIAA Aircraft Systems and Technology Meeting, Dallas, TX, September 1976.

3. Myklebust, Arvid and Gelhausen, Paul, "Putting the ACSYNT on aircraft design", Aerospace America, September 1994, pp. 27-29.

4. Gloudemans, James R., Davis, Paul C., and Gelhausen, Paul A. "A Rapid Geometry Modeler for Conceptual Aircraft", AIAA 96-0052, in AIAA 34th Aerospace Sciences Meeting and Exhibit, Reno, NV, January 1996.

5. Schmit, L.A. and Miura, H., "Approximation Concepts for Efficient Structural Analysis", NASA CR-2552, March 1976.

6. Bil, C., Van Dalen, F., Rothwell, A., Arendsen, P., and Wiggenraad, J.F.M., "Structural Optimization in Preliminary Aircraft Design: A Finite Element Approach", ICAS-92-6.7R2, Proceedings of ICAS, 1992, pp.1505-1515.

7. Haftka, R.T. and Gurdal, Z., "Elements of Structural Optimization", Third Revised and Expanded Edition, Kluwer Academic Publishers, Dordrecht, Boston, New York, 1992.

8. Felippa, C.A., "Solution of Linear Equations with Skylined Stored Symmetric Matrix", Computers and Structures, Vol. 5, No. 1, 1975, pp.13-29.

9. Daryl L. Logan, A First Course in the Finite Element Method, PWS Engineering, 1986.

10. Appa, K., "Finite-Surface Spline", Journal of Aircraft, Vol. 26, No. 5, pp.495-496, May 1989.

11. Hartley Grandin, Jr., Fundamentals of the Finite Element Method, Waveland Press, Inc., 1986.

12. Botkin, M.E., "Three Dimensional Shape Optimization Using Fully Automated Mesh Generation", AIAA Journal, Vol. 30, No. 7, July 1992, pp.1932-1934.

13. Stephen P. Timoshenko and James M. Gere, Theory of elastic Stability, McGraw-Hill, 1961.

14. Bruhn, Analysis and Design of Flight Vehicle Structures, Tri-State Offset Company, 1973.

15. David J. Peery and J.J. Azar, Aircraft Structures, Mcgraw-Hill, 1982.

16. Ashton and J.M. Whitney, Theory of Laminated Plates, Technomic Publishing Co., Inc., Stamford, CN, 1970.

17. Starnes, James H. And Haftka, Raphael T., "Preliminary Design of Composite Wings for Buckling, Strength, and Displacement Constraints", Journal of Aircraft, Vol. 16, No. 8, August 1979, pp.564-570.

18. Ragon, S.A., Gurdal, Z., and Starnes, J.H. Jr., "Optimization of Composite Box-Beam Structures including the Effects of Subcomponent Interaction", AIAA-94-1410-CP, 1994, pp.818-828.

19. Raphael T. Haftka, Zafer Gurdal and, Manohar P. Kamat, Elements of Structural Optimization, Kluwer Academic Publishers, 1990.

20. Schmidt, L.A. and Mehrinfar, M., "Multilevel Optimum Design of Structures with Fiber-composite Stiffened Panel Components", AIAA Journal, Vol. 20, No. 1, June 1982, pp. 138-147.

21. Suzuki, Shinji and Yonezwawa, Satoshi, "Simultaneous Structure/Control Design Optimization of a Wing Structure with a Gust Load Alleviation System", Journal of Aircraft, Vol. 30, No. 2, April 1993, p.268.

22. Kajiwara, I., Tsujioka, K., and Nagamatsu, A., "Approach for Simultaneous Optimization of a Structre and Control System", AIAA Journal, Vol. 32, No. 4, April 1994, p.866.

23. Schmidt, L.A. Jr. and Ramanathan, R.K., "Multilevel Approach to Minimum Weight Design including Buckling Constraints", AIAA Journal, Vol. 16, No. 2, February 1978, pp. 97-104.

24. Garret N. Vanderplaats, Numerical Optimization Techniques for Engineering Design: with Applications, McGraw-Hill, 1984.

25. Bartholomew, Peter, Harris, John, and Weillen, Heinrich, "The Integration of Local Design of Composite Panels into the Overall Structural Design", AIAA-94-4354-CP, 1994, pp.957-965.

26. Wakayama, Sean, "Wing Weight Estimation", Stanford University, March 1993.

27. Volk, J.A., Ausman, J.D., and Tich, E.J., "The Role of Automated Multidisciplinary Structural sizing in Flexible Wing Development", AIAA94-1485, in proceedings of the 35th AIAA/ASME/ASCE/ASE Structures, Structural Dynamics, and Materials Conference, Hilton Head, SC, April 1994.

28. Ausman, J.D., Hangen, J.A., and Acevedo, D.A., "Application of a Local Panel Buckling Constraint Within Automated Multidisciplinary Structural Analysis and Design", AIAA 92-1116, in prceedings of 1992 Aerospace Design Conference, Irvine, CA, February 1992.

29. George I.N. Rozvany, Structural Design via Optimality Criteria: The Prager Approach to Structural Optimization, Kluwer Academic Publishers, 1989.

APPENDIX A
CDOSS PROGRAM INFORMATION

A.1 Introduction

This appendix contains user information for CDOSS, the code developed and used in this thesis. The subroutines are briefly described and grouped by function. The program structure is outlined and main program variable are described. All programs and subroutines are written in FORTRAN.

A.2 Program Subroutines

Intfem is the main program. Geometry of the wing is defined here.

Mesh Generation:

- Interpol - interpolates points between ACSYNT provided points
- Renum - renumbers the points for convenience
- Element - creates elements for finite element model
- Shape - transforms aerodynamic loads using shape functions
- Cheb - transforms aerodynamic loads using chebychev functions
- Fload - calculates equivalent point loads for uniformly distributed loads or tip loads

Panel Generation:

- Panelid - identifies the panel nodes and membranes
- Panelch - finds the dimensions and sweep of each panel
- Panelst - calculates panel average thickness, stress, and nodal forces

F1fem is the subroutine that performs the analysis and optimization.

The following subroutines are called within F1fem.

Getdata is a subroutine that reads finite element data (nodes and elements).

Stiffness Matrix:

Ske - computes elemental stiffness matrix for truss elements

Kmerge - adds truss element stiffness matrix to global stiffness matrix

Skm - computes elemental stiffness matrix for membrane elements

Lmerge - adds membrane element stiffness matrix to global stiffness matrix

Skyfac/Skysol solve linear equations using the method of reference 4.

Elemental Stress:

Stre - computes truss element stress

Strm - computes membrane element stresses

Buckling:

Transform - transforms global stresses to local coordinates

Critical - calculates buckling constraint values for all constrained elements

Critopt - calculates buckling stress and constraints for wing skin only

Geom calculates the geometric characteristics of the elements.

Final outputs the results of the optimized model.

There are also small subroutines that perform basic matrix manipulations.

A.3 Program Structure

A brief description of the structure of the program and the major variable within each section will be described.

Wing Geometry and Mesh Generation:

In this section, data is gathered from ACSYNT and from the user for wing geometry. The finite element mesh is then generated.

Gather Data:

herm(comp#,section#,point#,direction) - cross sectional data from ACSYNT

sparcon - choice of spar configuration

nspar - # of spars at the root

nrib(section#) - # of ribs in the section

bshape - wing box shape

lp,tp - % chord for slats and flaps

sthick,rthick - spar and rib web thickness

area1,area2 - spar and rib cap area

Create Elements:

nnx - # of nodes in the x direction

nny - # of nodes in the y direction

upsurf - # of membrane elements on the upper surface

xc,yc,zc(node#) - coordinates of nodes

nnodes - total # of nodes

mem(vertice#,membrane#) - membrane node data

node(vertice#,truss#) - truss node dataa

th(membrane#) - membrane thickness

ax(element#) - truss element area

force(direction,node#) - applied nodal force

ifix(direction,node#) - boundary conditions

dum(dummy node#) - node number of a dummy node

Panel Identification:

In this section, panels are identified and panel characteristics are calculated.

paneln(panel#,vertice#) - nodes at panel vertices

panelm(panel3,membrane#) - membranes in each panel

npanel(3) - # of panels in wingskin, rib webs, or spar webs

panelth(panel#) - average thickness of panel elements

pstress(panel#,direction) - average stresses in panel

nforce(panel#,node#,direction) - nodal forces

sweep(panel#) - sweep of panel

apan,bpan(panel#) - dimensions of panel

Material Properties:

In this section, the user inputs the material propertied needed for analysis.

ex - elastic modulus for truss elements

rho1 - density of truss elements

amin,amax - minimum and maximum allowable area

em - elastic modulus for membrane elements

rho2 - density of membrane elements

pr - Poisson's Ratio

tmin,tmax - minimum and maximum allowable thickness

sf - safety factor

yield - yield strength

tol - convergence criteria tolerance

Stress Analysis:

Here the stiffness matrix is formed and the stresses calculated.

skele - truss elemental stiffness matrix

skmem - membrane elemental stiffness matrix

stifk - global stiffness matrix

disp(direction,node#) - nodal displacements

str(truss#) - truss element stress

smem(direction,membrane#) - membrane element stresses

force2(node#,direction) - local forces

Optimization:

In this section, the optimization if performed, weight is calculated and convergence is checked.

iter - iteration number

cstr1 - buckling constraint value

equiv - equivalent stress

tratio - ratio of equivalent stress multiplied by safety factor and of yield stress

thnew(membrane#) - new skin thickness

obj(iteration#) - mass after optimizing

rmax - largest constant violation

Following the optimization routine, the stresses are calculated again based on the new thickness. If the weight does not converge, then the routine returns to the optimization loop.

A.4 Node and Element Numbering

A description of the node and element numbering follows. The nodes are numbered on the upper surface then the lower surface. The first node is at the leading edge of the root chord. The nodes are then numbered along the chord to the trailing edge. Numbering continues in this manner for each chord from the root to the tip. Figure A1 illustrates this numbering scheme. Membranes are numbered in the same order as nodes. The upper skin is first followed by the lower skin. Rib webs are numbered next, then spar webs. Truss elements begin with spar caps on the upper, then lower surface. Vertical spacers are numbered next. Rib caps are then numbered, alternating from upper to lower surface for each rib section. (See figure A1) Buckling panels are numbered in the same order as membrane elements.

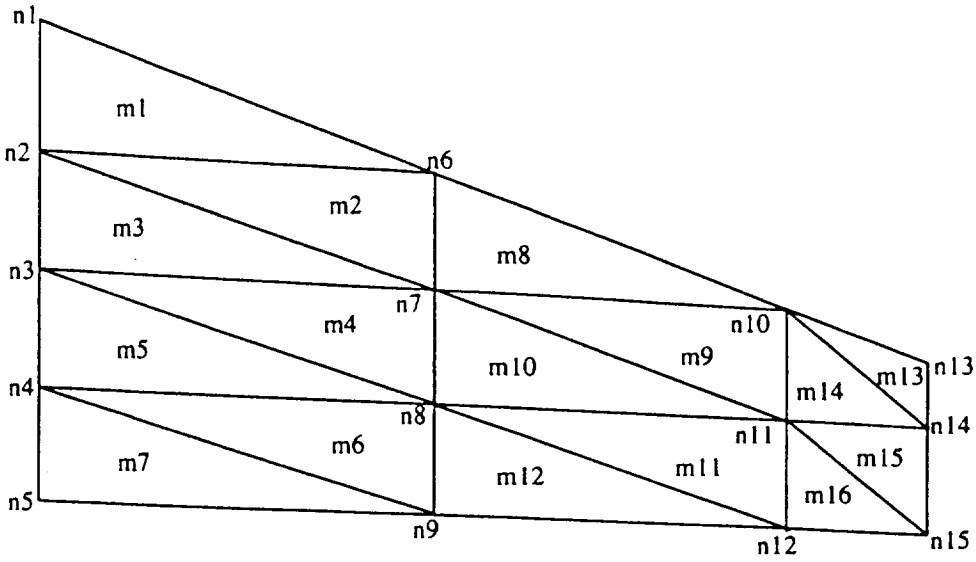

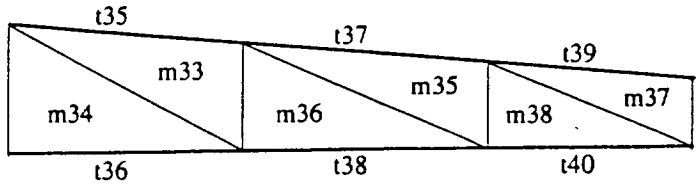

rib

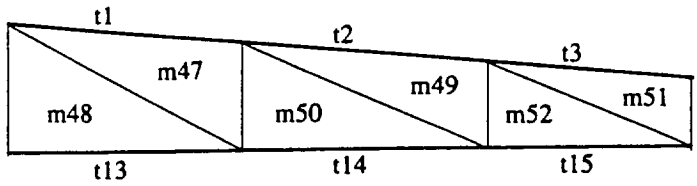

spar

n# - indicates node number

m# - indicates membrane number

t# - indicates truss number

Figure A1. Node and Element Numbering

Thesis Addendum

May Y. Lau

December 1996

Point Loads:

Point loads for fuel, engines, external stores, etc. Can be specified in a data file. The location of the point load must be specified within the geometry of the wing box. Shape functions are used to distribute the load to nodes of the cell which the point is located. Sum of forces and moments are conserved.

Aerodynamic Loads:

The aerodynamic loads which do not lie in the wing box are not included in the transformation of aerodynamic loads to structural points. These loads are placed at the nearest nodes along the leading or trailing edge. This method does not account for the change in moments. The change in moments could be dealt with by adding couple on the wing.

Uniformly Distributed Load:

CDOSS uses the gross weight estimate and the number of 'g's of the maneuver to calculate the distributed load. The gross weight multiplied my the number of 'g's is spread uniformly over the wing box area. These forces are then lumped onto the nodes based on the amount of area around each node.

Natural Frequencies:

To find natural frequencies of a wing, it is necessary to find the eigenvalues of the system. The general equation of motion is $[-\omega^2 M + K]\{\phi\} = \{0\}$ where ω is the natural frequency, M is the mass matrix, and K is the stiffness matrix, and ϕ is the vector of displacements. The eigenvalue solver solves equations of the form $[A - \lambda I]\{x\} = \{0\}$ where I is the identity matrix. The equation of motion can be manipulated into this form.

$$[-\omega^2 M + K]\{\phi\} = \{0\}$$

$$\left[-\omega^2\sqrt{M}\sqrt{M} + K\right]\{\phi\} = \{0\}$$

$$\sqrt{M}^{-1}\left[-\omega^2\sqrt{M}\sqrt{M} + K\right]\{\phi\} = \{0\}$$

$$\left[-\omega^2\sqrt{M} + \sqrt{M^{-1}}K\right]\{\phi\} = \{0\}$$

$$\text{let } \{\phi\} = \sqrt{M}^{-1}\{\xi\}$$

$$\left[-\omega^2\sqrt{M} + \sqrt{M^{-1}}K\right]\sqrt{M}^{-1}\{\xi\} = \{0\}$$

$$\left[-\omega^2 I + \sqrt{M^{-1}}K\sqrt{M}^{-1}\right]\{\xi\} = \{0\}$$

$$\text{let} \quad \lambda = \omega^2$$

$$A = \sqrt{M^{-1}}K\sqrt{M}^{-1}$$

$$[A - \lambda I]\{\xi\} = \{0\}$$

The stiffness matrix is already formed for the stress analysis. The mass matrix is created by a simple lumped mass method. The weight of all structural elements are summed and lumped at nodes. No dynamic or external masses are included. The

mass matrix is a simple diagonal matrix. The inverse square root if this matrix is simply the reciprocal of the square root of the diagonal elements. The multiplication is carried out to obtain the A matrix. The eigenvalue solver finds the eigenvalues of A. To obtain natural frequencies in units of hertz, simply divide the square root of the eigenvalue by 2π.

$$\omega(hertz) = \frac{\sqrt{\lambda}}{2\pi}$$

The natural frequencies can be used for flutter analysis.

Input and Output Files:

Input Files (in units of feet, lbs, etc.):

Geometry file - f16

- gross weight
- number of components
- number of cross-sections
- number of points per cross-section
- list of points: x, y, and z coordinates

Design data file - wingdata

- spar configuration
- number of spars
- number of ribs in section 1, section 2, etc.
- wing box shape
- percent chord for slats and flaps
- wingskin thickness at root and tip
- spar and rib web thickness
- spar and rib cap area

percent thickness for dummy webs

vertical spacer area

load choice

aerodynamic transformation method or number of 'g's of maneuver

filename of aerodynamic loads

point loads, yes or no

filename of point loads

optimize, yes or no

elastic modulus and density of bars

minimum truss area

maximum truss area

elastic modulus, poisson's ratio, and density of membranes

minimum thickness of membranes

maximum thickness of membranes

step size for buckling optimization

type of loading for membranes

design safety factor

material yield strength

convergence criteria tolerance

Aerodynamic Loads file - f16load

- number of points
- list of points: x, y, and z coordinates, vertical force

Point Loads file - ptloads

number of points

list of points: x, y, and z coordinates, vertical force

FEM files - wingtemp and opt.f16

filename

number of nodes, truss elements, and membrane elements

list of nodes: node number x, y, z coordinates, x, y, z forces

list of truss elements: element number, node 1, node 2, area

list of membrane elements: element number, node 1 thru 3, thickness

Displacement Output - out.f16

list of displacements: node number, x, y, z displacements

list of truss element stresses: element number, stress

list of membrane stresses: element number, principle stresses, shear stress

Buckling Output - out.buckle

list of panels: panel number, buckling constraint value

list of truss elements: element number, buckling constraint value

list of eigenvalues